NATIONAL AERONAUTICS AND SPACE ADMINISTRATION
Washington, D. C.

NASA Grant NGL 44-012-006

THIRD QUARTERLY PROGRESS REPORT

1 October 1969 - 31 December 1969

Submitted by

Electrical Engineering Research Laboratory
MILLIMETER WAVE SCIENCES
The University of Texas at Austin
Austin, Texas

Third Quarterly Progress Report Under
NGL 44-012-006 for the Period from
1 October 1969 - 31 December 1969

I. Introduction

This progress report covers the work performed under NGL 44-012-006 for the period 1 October 1969 to 31 December 1969. This period was very significant in the overall program of radio astronomy at the Millimeter Wave Observatory, Mt. Locke, Texas, in that it marked the dividing line between the basically engineering program of antenna evaluation and the basic astronomical observing program to which the facility is committed.

In this report we discuss the work under the usual headings of engineering and astronomy. The engineering section is concerned mainly with work on the receivers in use on the radio telescope. The astronomy portion describes analytical work on the 11 September 1969 solar eclipse measurements as well as the beginnings of a planetary observing program.

II. Engineering Work

The major event in the antenna evaluation program was the reshimming of the antenna structure in the summer of 1969. This work increased the antenna efficiency from 34% at a frequency of 95.0 GHz with 12 dB sidelobes to 43% at 134.0 GHz with 21 dB sidelobes.

The effect of this improvement in antenna performance was to create an urgency in equipping the receivers for astronomical use as well as in refining pointing corrections, generating ephemerids: in short, in dealing

with the remaining obstacles to full time use of the telescope in astronomical observations.

The major work was in getting the receivers prepared for astronomical observations. Early in the summer, when things begin to look up for the antenna, the needed parts for adding calibration circuitry were ordered. By mid-October everything had arrived and the calibration circuitry was constructed.

Meanwhile, the digital data system, which went out for bids in March, arrived at Mount Locke. This equipment digitizes, formats, and serializes the data and punches it on paper tape. The system had a few malfunctions in its first weeks of use but these were repaired and it has proven on the whole well conceived for its role.

The final step in readying the receiver systems was calibrating them in thermal units. During observations, the receivers are calibrated by firing a noise tube into a reference port. The thermal equivalent of the resulting signal was determined by reference to a temperature controlled "black-body" (actually, a well-matched waveguide termination), which replaced the feed for this test. Thus all astronomical measurements are in effect calibrated with respect to a thermal reference. Repeated calibrations indicated a 5% random error for this method. Systematic errors are more difficult to judge. A 7% accuracy will be assumed in data analysis.

These tests also yielded a direct evaluation of the receiver sensitivity. The results are shown in Table I below.

ν(GHz)	ΔT_{rms} (τ = 1 sec)
35	1°K
97	7°K
140	20°K

Table I Receiver Sensitivity

These figures show that the receivers are not near the state-of-the-art, although they do allow a basic program of solar system radio astronomy. In the next section we describe the beginnings of such a program.

In preparation for the observing program, we completed the pointing calibrations. This program was the subject of our Technical Memorandum No. NGL-006-69-3 entitled "Pointing of the 16 Foot Antenna." Our approach to the pointing problem is basically to evaluate and correct for all the errors in the production of an observing ephemeris. Corrections for sag, r.f. refraction, axis tilts, and encoder errors are used. Data are taken by the drift scan method with the antenna stationary, which leads to the simplest observing procedure. One by-product of this pointing evaluation was a better measurement of r.f. refraction than was currently available. These results have been accepted for publication. The final draft of our paper appears in Appendix A of this report.

III. Astronomy

During the reporting period, analysis was being done on the data taken during the partial solar eclipse of 11 September. This work was done in

cooperation with the other millimeter observatories in the country. The basic experiment was suggested by Dr. Michal Simon of The University of New York at Stony Brook, and was designed to measure the solar limb distribution through occultation by the lunar limb.

Most of the models proposed for the quiet sun radiation at millimeter wavelengths predict some amount of limb brightening. Measurements in search of this effect have been inconclusive: our own data taken by the drift scan method, for example, appear to indicate a flat distribution near the limb.

In this experiment, we tracked the solar limb at the first and fourth contact points and allowed the moon to move across the beam, thus extinguishing the solar limb radiation in a predictable manner. The advantage of this method is that anomalies, e.g., a ring of excess radiation at the limb, would show up in the extinguishing curve.

The weather for the eclipse was excellent, but the data were very noisy. The noise was traced to seeing effects rather than to receiver noise. Figure 1 and figure 2 shows the data for both contacts. The flat portions are the tracks of the limbs, and the decreasing portions are caused by the motion of the moon across the antenna beam.

The data were analyzed by fitting a straight line to the limb track portion, fitting an error function to the extinguishing portion, and extrapolating these curves to the point of contact. The fitted lines are shown on Figures 1 and 2. Several features of these data deserve mention. Notice that the data are more noisy during the limb tracking portion of

the data. This is due to a seeing phenomena; these data indicate a seeing motion of the solar image of approximately 12 arc sec, rms. (This is a different seeing parameter than is used in astronomy.) Another interesting feature of the data is the slope of the curves in the limb track portions. This is an indication of a loss of signal as the moon obscures the lower corona, and hence indicates some millimeter radiation in this region.

A discontinuity between the two curves in Figures 1 and 2 would indicate an excess of radiation at the limb. Our results indicate, however, that no such discontinuity exists and we conclude that the distribution is flat to the optical limb, where it drops abruptly to a value near the sky value. We might mention in conclusion that we are currently preparing to repeat the experiment during the 7 March eclipse so as to improve the signal-to-noise ratio.

In 1967-1968, Dr. Takashi Yamashita of The Research Institute of Astrophysics, Nagoya University, was resident at the Millimeter Wave Observatory. Although Dr. Yamashita's chief interest was solar radio astronomy, he did work in other areas while in Texas. Some of his work on sky emission phenomena and the polarization of lunar radiation have appeared in the Proceedings of the Research Institute of Atmospherics, Nagoya University, Vol. 17A (January 1970), pp. 1-52. The published material is included herein as Appendix B.

The other major activity under this heading was the establishing of an observing program. This required essentially defining priorities and designing an observing procedure compatible with the ephemerids and data recording facilities available.

The planets available for observation in December were Jupiter and Saturn. Although Jupiter offered a larger signal, Saturn was getting farther away and Jupiter was coming nearer. For this reason we decided to begin with Saturn and to observe Jupiter second. Only a few observing days were left in December but some ten days observations have been made at the time of writing.

The observing procedure is basically a drift scan approach, with calibrations and extinction scans of the sun included to allow accurate data reduction. The details of this procedure are of little interest here.

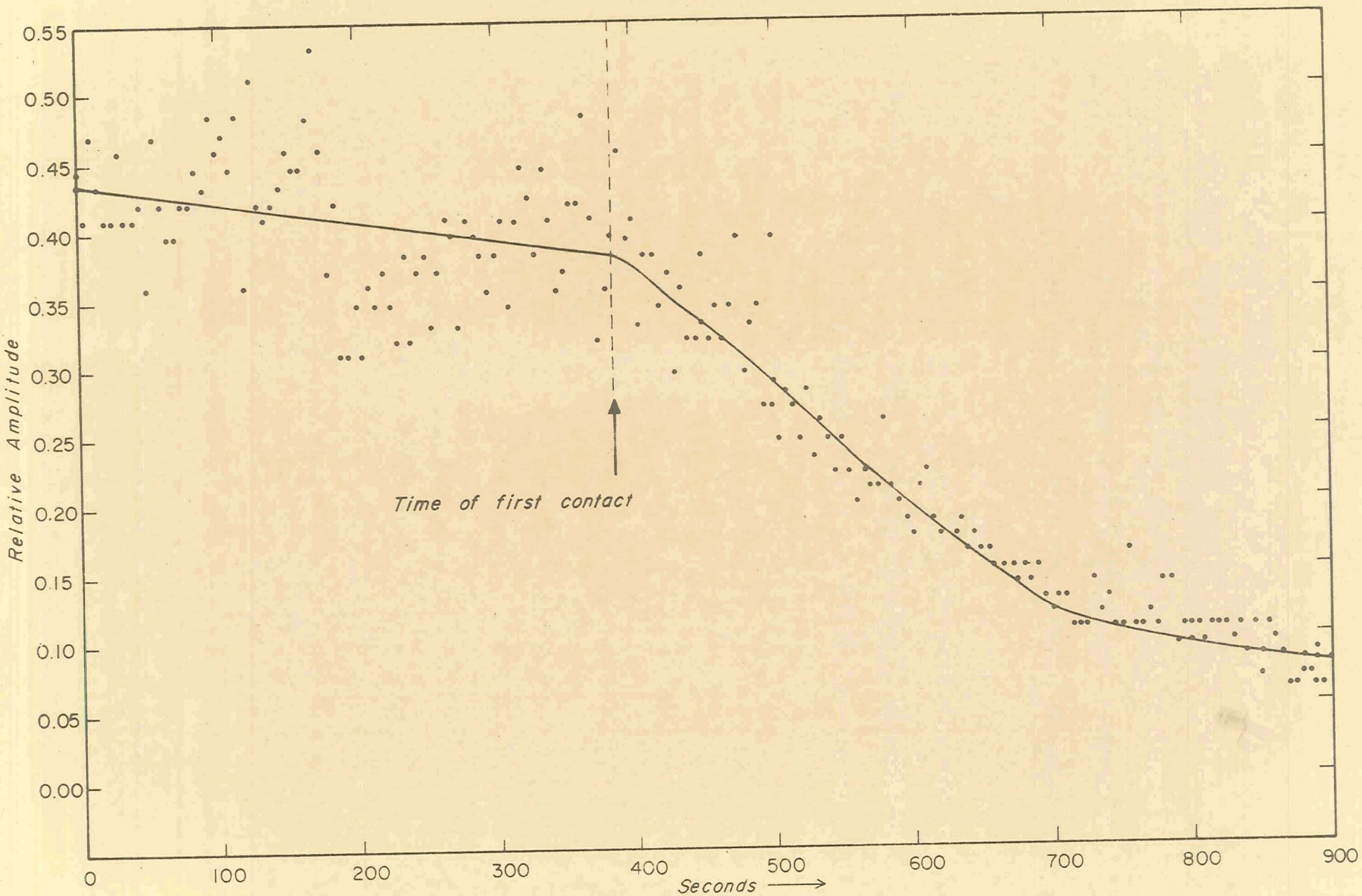

Fig. 1. FIRST CONTACT DATA

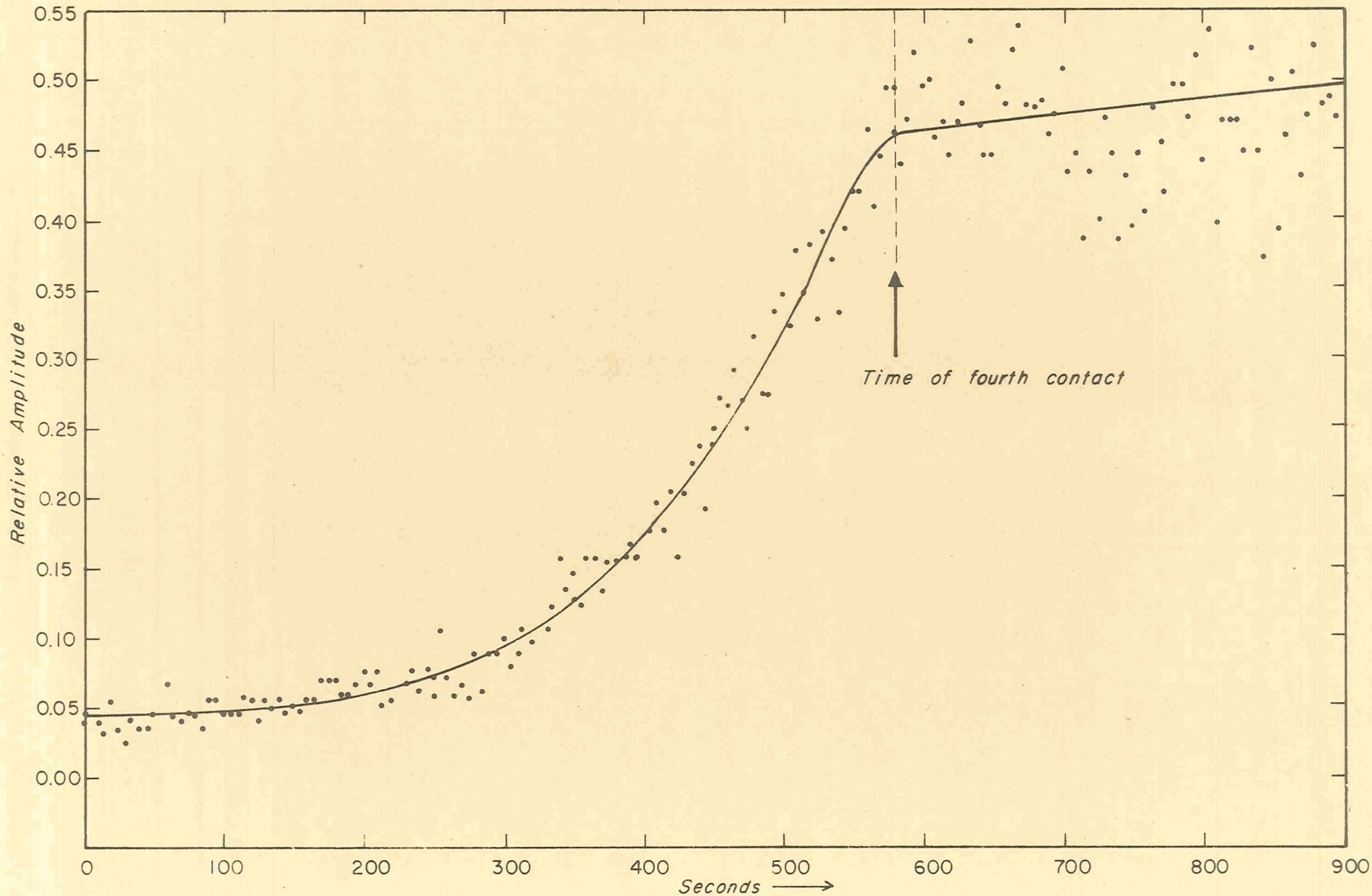

Fig. 2. FOURTH CONTACT DATA

APPENDIX A

Astronomical Refraction at Millimeter Wavelengths

John H. Davis, Dept. of Electrical Engineering
John R. Cogdell, Electrical Engineering Research Laboratory
The University of Texas at Austin

I. Introduction

This paper reports measurements of astronomical refraction at wavelengths of 8.6 mm (35 GHz), 4.3 mm (70 GHz), 3.1 mm (97 GHz), and 2.17 mm (134 GHz). Taking the viewpoint that knowledge of optical astronomical refraction is well established in theory and practice, we have made measurements of differential refraction between optical and radio frequency (r.f.) waves as they pass through the atmosphere. These measurements are a small part of a larger calibration program at the Millimeter Wave Observatory, Mt. Locke, Texas.*

These measurements have practical importance for the use of high resolution antennas in and through the atmosphere in that refractive pointing corrections can be comparable to beamwidths at low elevation angles. Also, since the surface refractive index determines the magnitude of the refraction effects, these measurements seem to widen considerably the frequency range within which the radio refractive index has been measured.[1]

The first measurements of astronomical refraction of microwaves were reported by Aarons, Barron, and Castelli.[2] They made low resolution studies at 3.2 cm and 8.7 mm and observed total refraction directly. Their results failed to demonstrate a direct proportionally between r.f. and optical.

*Operated by the Electrical Engineering Research Laboratory, The University of Texas at Austin under NASA Grant NGL 44-012-006.

refraction and exhibited wide day-to-day variability. Tolbert, Britt, and Bahn[3] made differential refraction measurements at 4.3 mm. Their results were of low resolution but generally showed the expected refraction curve. Anway[5] made extensive total refraction measurements and derived a semiempirical relation to fit the data.

In the following section we describe our measurement technique and data analysis procedures. We present our results in the following section and compare them with what the simple theory of refraction would predict. Our results support a simple theory of astronomical refraction at millimeter wavelengths, in that our data exhibit the expected geometrical and meteorological dependences.

II. Measurement Techniques

The measurements were made with the 16' radio telescope at the Millimeter Wave Observatory, Mt. Locke, Texas. The patterns of the antenna at 134 GHz are shown in Figure 1 and indicate near-theoretical performance at and below that frequency. The radio telescope is equipped with standard Dicke radiometer receivers at 35 GHz, 70 GHz, 97 GHz, and 134 GHz, and operates with the feed at the prime focus. The 3 dB beamwidth at 134 GHz is 0.033° and allows particularly high resolution measurements.

The differential refraction measurements were made by observing the transit of the solar limbs through the antenna beam. The optical limbs of the sun are observed through collimated optical telescopes and marked on the chart along with the receiver response. Both limb crossings are observed

in a drift scan and the optical and radio limb crossing times are averaged. The radio limb is identified as the point at which the response has risen to one-half its value on the solar disc.

At 8.6 mm, 4.3 mm and 3.1 mm, the sunrise can be observed from the horizon but at 2.17 mm atmospheric extinction and radiometer sensitivity combine to limit observations to elevation angles about 6°. The sun is observed in this fashion until it is high in the sky, ideally until meridian transit or after, in order to estimate and remove sag effects.

The data were analyzed in the following manner. A scan results in a data point

$$d_i = T_{rf} - T_{opt}$$

where d_i is the difference time between r.f. transit and optical transit of the sun in seconds. As the sun moves across the sky, d_i changes due to differential refraction, antenna sag, and geometric factors. The various factors are related through the equation[6]

$$K\, d_i \cos\delta = \{S \cos(E_i) - r\, R_o(E_i)\} \sin\mu_i + C$$

where

K = solar rate (deg./sec.)

δ = solar declination

S = antenna sag, zenith to horizon (deg.)

E_i = antenna elevation angle for i^{th} data point

r = differential refraction

$R_o(E)$ = Garfinkel optical refraction function[7]

μ_i = angle between sun's path and horizontal line

C = constant of no importance in this work.

For each day's data, r, S, and C are regressed to the data according to the equation given. Typical data, with the best fit curves, are shown in Figures 2 and 3. The parametric equation fit to the data was confirmed experimentally by varying the sag term. When weights were hung on the antenna feed structure, the sag coefficient in the equation varied greatly while the refraction coefficient was unchanged. Figure 2 displays data where the sag term is large. Figure 3 shows a data set where sag is small. In either event, the sag term does not naturally couple the refraction term.

The errors in the data are due to radiometric noise, differential seeing effects, and operator inaccuracy in marking the optical limbs. The effect of these errors on the accuracy of the estimate of r was determined by generating data sets on a digital computer and regressing the parametric equation to a number of such data sets. This procedure was followed for each day's measurement, since the exact position and number of data points are significant.

III. Results

A large number of data sets were obtained during the antenna calibration program to measure sag and opacity, but only a few of these were carried to elevation angles which were low enough to allow accurate evaluation of differential refraction. Table 1 gives selected data with meteorological

Date	λ (mm)	T_{amb}	R.H.	P	Measured $r \pm \sigma_r$	Theoretical r
23 July 1969	8.6	61°	56%	23.5	0.13±.02	0.200
31 July 1969	8.6	61°	43%	23.5	0.16±.02	0.150
4 Dec 1969	8.6	41.3°	95%	23.5	0.16±.01	0.180
July 1968	4.3	--	--	--	0.20±.04	--
1 Dec 1969	3.1	40°	82%	23.5	0.17±.01	0.140
27 Aug 1969	2.2	57°	100%	23.5	0.25±.02	0.334
5 Oct 1969	2.2	68°	47%	23.6	0.16±.02	0.222
6 Oct 1969	2.2	67°	95%	23.7	0.24	0.326

Differential Refraction Measurements

Table 1

conditions. The meteorological data given in Table 1 were recorded from inexpensive instruments and are probably not highly accurate. The data accuracies, σ_r, are standard deviations.

The simple formula for radio refractive index is

$$N = \frac{77.6\ P}{T}\left[1 + \frac{4810}{T}\left(\frac{e}{P}\right)\right]$$

where T, P, and e, are the temperature (°K), pressure (mb), and partial pressure (mb) due to water vapor.[1] The second term in this equation represents the difference between optical and radio refraction. The simple theory of astronomical refraction shows that the total refraction depends only upon the surface refractive index[8] term. Figure 4 shows our data plotted against the term discussed above. The solid line gives the dependent the simple theory would suggest. We feel that in view of the relative crudeness of the meteorological measurements, our data are compatable with the simple theory up to 100 GHz. However, at 134 GHz the data fall significantly below the theoretical line in favor of the optical refraction values. This is an expected result since the polarization experiences a downward break somewh ere above 100 GHz.[9] Our results indicate that this break occurs between the 100 GHz window and the 140 GHz window.

References

1. Bean, Bradford R., "The Radio Refractive Index of Air," Proc. IRE, Vol. 50, No. 3 (March 1962), pp. 260-273.

2. Aarons, J., W. R. Barron, and J. P. Castelli, "Radio Astronomy Measurements at VHF and Microwave," Proc. IRE, Vol. 46, No. 1 (January 1958), pp. 325-333.

3. Tolbert, C. W., Chester Britt, and W. Bahn, Technical Report No. 103, Electrical Engineering Research Laboratory, The University of Texas, (1958). Their differential refraction curve appears in Ref. 4.

4. Tolbert, C. W., L. Krause, and A. W. Straiton, "Solar Radiation at 3.2 mm During 20 July 1963 Eclipse," Ap. J., Vol. 140 (1964), p. 310.

5. Anway, A. C., Collins Radio Report CRR 242S.

6. Davis, John H. and John R. Cogdell, "A Pointing Study of the 16-Foot Antenna," Electrical Engineering Research Laboratory, The University of Texas at Austin, Technical Memorandum No. NGL-006-69-3 (1969).

7. Garfinkel, B., "An Investigation in the Theory of Astronomical Refraction," Astronomical Journal, Vol. 50 (1944), p. 196.

8. Blanco and McCuskey, Basic Physics of the Solar System, Addison-Wesley Publishing Company, Inc., Reading, Massachusetts (1961), p. 91.

9. Bean, op. cit., p. 260 f.

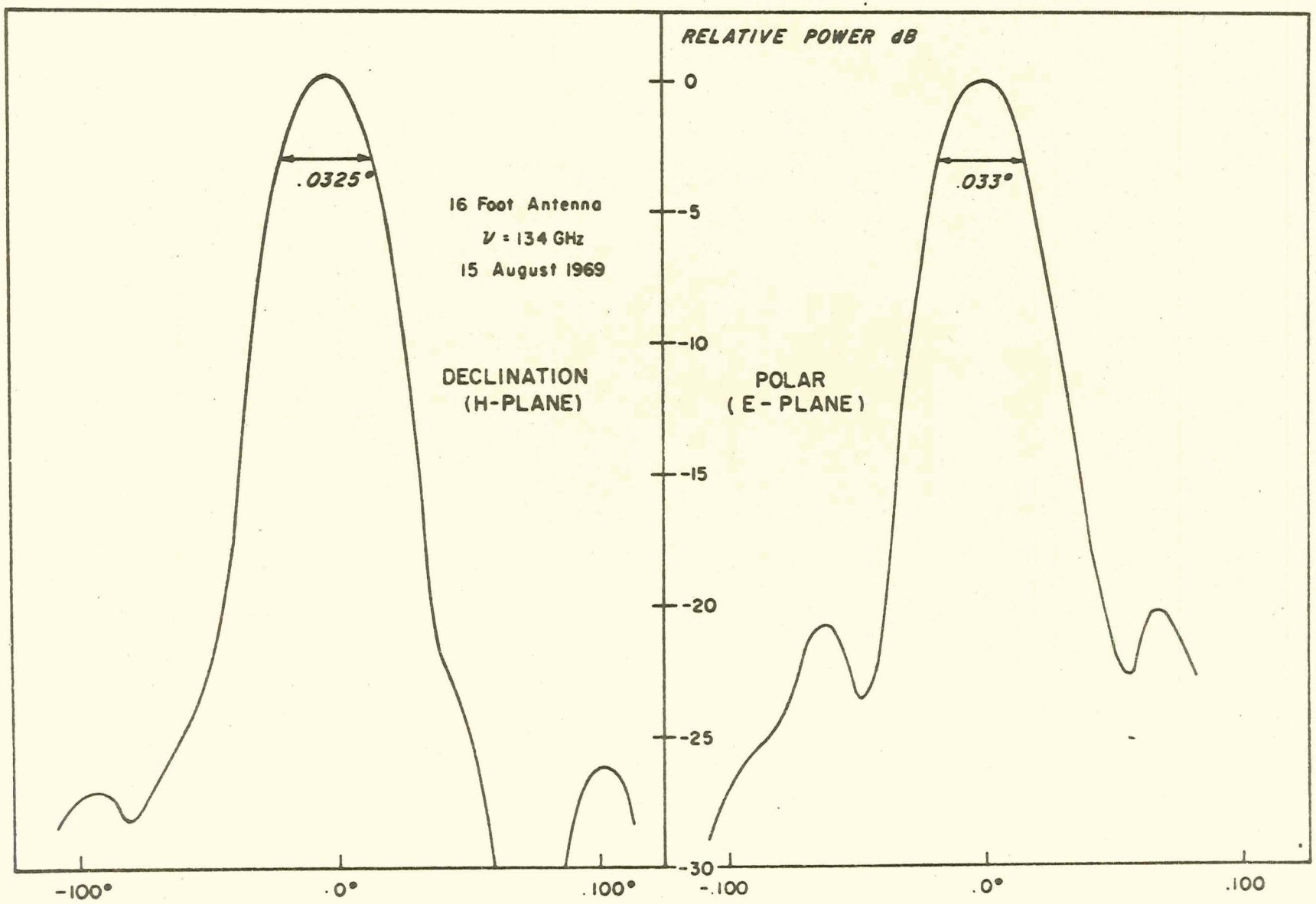

PATTERNS AT $\nu = 134$ GHz

FIG. 1

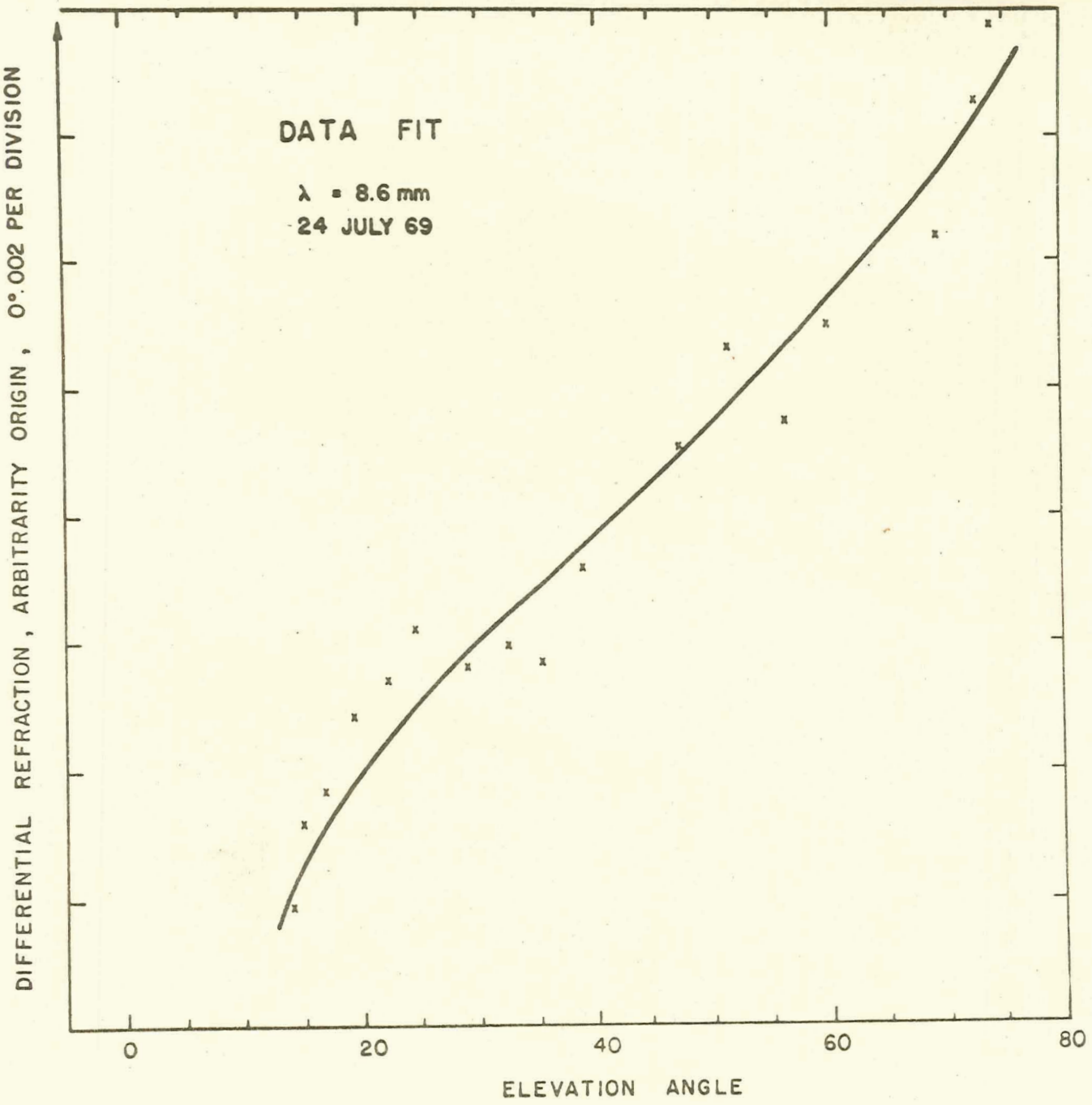
DATA FIT
λ = 8.6 mm
24 JULY 69
DIFFERENTIAL REFRACTION, ARBITRARITY ORIGIN, 0°.002 PER DIVISION
0
20
40
60
80
ELEVATION ANGLE

FIG. 2

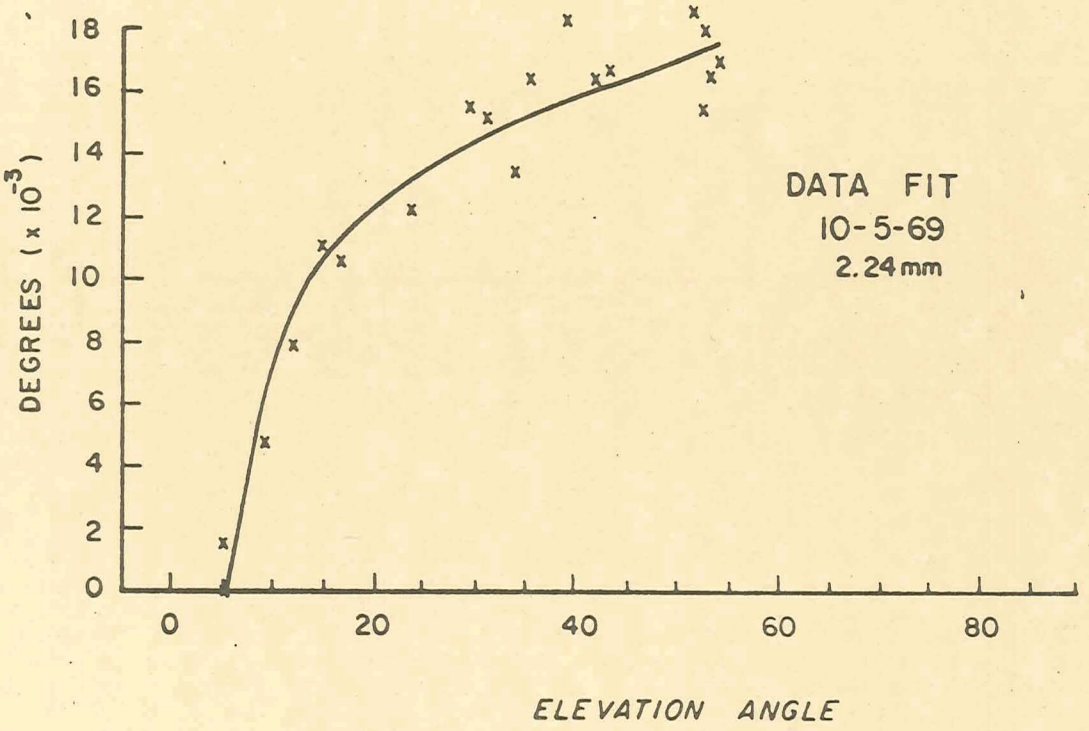
DEGREES (x 10^-3)
18
16
14
12
10
8
6
4
2
0
0
20
40
60
80
ELEVATION ANGLE
DATA FIT
10-5-69
2.24 mm

FIG. 3

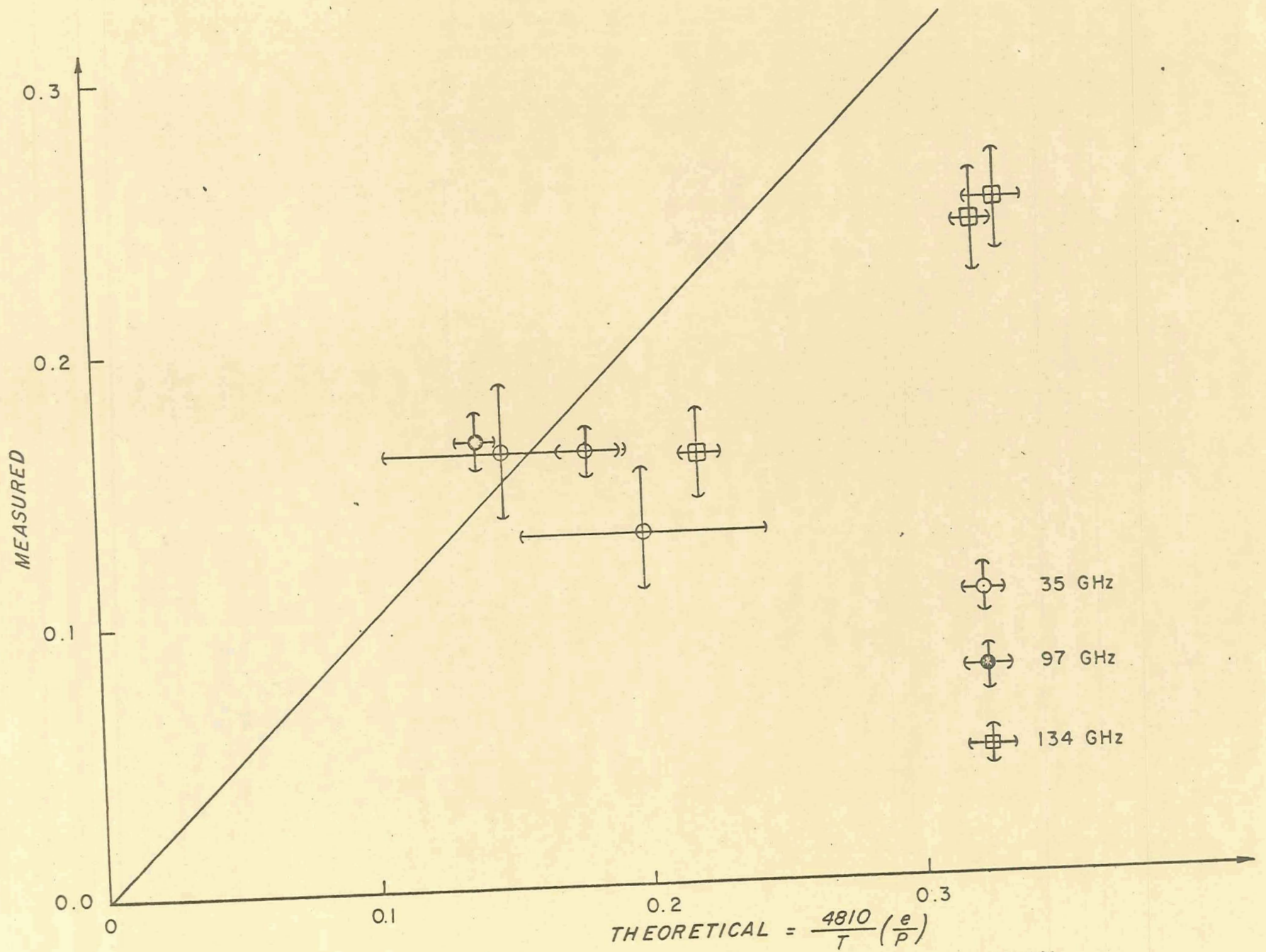

Fig. 4. MEASURED VS THEORETICAL REFRACTION

APPENDIX B

TIME-DEPENDENT VARIATIONS IN SKY EMISSION TEMPERATURES AT AT MILLIMETER WAVELENGTHS

ANOMALOUS SKY TEMPERATURE VARIATION WITH ZENITH DISTANCE MEASURED AT A CALM NIGHT AT A WAVELENGTH OF 3.2 MM.

MEASUREMENTS OF LINEAR POLARIZATION OF THE MOON AT MILLIMETER WAVELENGTHS

TAKASHI YAMASHITA

Proceedings of
the Research Institute of Atmospherics
Nagoya University

Vol. 17. A. January 1970

CONTENTS

Time-Dependent Variations in Sky Emission Temperatures at Millimeter Wavelengths. 1

Anomalous Sky Temperature Variation with Zenith Distance Measured at a Calm Night at a Wavelength of 3.2 mm. 29

Measurements of Linear Polarization of the Moon at Millimeter wavelengths 34

ACKNOWLEDGEMENT

The papers presented here are based on the results of observations performed by the auther during his stay at Millimeter Wave Sciences, Electrical Engineering Research Laboratory, The University of Texas in 1967-1968.

The hospitality given to the auther by the University and its staff is gratefully acknowledged. In particular it is a pleasure for this auther to thank Professor A. W. Straiton, Director of Electrical Engineering Research Laboratory for his continuous encouragement and deep interest in the works performed by the auther during his stay at the Millimeter Wave Observatory at Mt. Locke for one year. Thanks are also due to Dr. J. R. Cogdell of EERL for his encouragement and kindness in supporting the auther to perform the observations reported here.

The auther is deeply indebted to Mr. C. W. Tolbert who was responsible for the design of the 16-foot diameter millimeter wavelength telescope used in the observations.

The auther would also like to express his gratitude to Messrs. W. Bahn, T. Walker, T. Boone, and R. Tilley of Millimeter Wave Sciences of EERL for their aid in facilitating the observations for him.

The auther expresses his sincere thanks to Professor S. Ueno of the Institute of Astrophysics, University of Kyoto for incessant encouragement, discussions, and guidance. He is also

indebted to Professor S. Miyamoto, Director of Kwasan Observatory of University of Kyoto for fruitful discussions on the lunar surface structure, and to Dr. I. Kawaguchi of the Institute of Astrophysics, University of Kyoto for his discussions on the solar influence on the earth's atmosphere.
Warm consideration and encouragement of Professor H. Tanaka of the Research Institute of Atmospherics, Nagoya University for the auther in facilitating the study of the observational data for the present papers are gratefully acknowledged.
Thanks are also due to Mr. T. Takayanagi who helped the auther in preparing the figures in the papers, and to Miss K. Yamamoto who typed the manuscripts.
These researches were supported under NASA Grant NGL 44-012-006.

TIME-DEPENDENT VARIATIONS IN SKY EMISSION TEMPERATURES AT MILLIMETER WAVELENGTHS

Abstract---In this paper time-dependent variations in sky emission temperatures at millimeter wavelengths are reported. In the course of the observation of the Crab nebula, a constant increase in sky background emission was noticed. Measurements of zenith emission at wavelengths of 8.6 and 3.2 mm indicated that the sky emission temperature increased gradually through the early morning hours until it attained a maximum at around an hour before ground sunrise. After this maximum the sky emission decreased rapidly. The arrival of the maximum is likely to have a wavelength dependence. Possible mechanisms for the phenomena are suggested and the diurnal and seasonal variations in the sky emission temperatures inferred from the analyses of the phenomena are also presented.

1. Introduction

Millimeter wave attenuation and emission are primarily controlled by the atmospheric temperature, molecular oxygen, and water vapor. The well-known Van Vleck-Weisskopf equation [1, 2, and 3] gives approximate values of attenuation and emission by the aid of an appropriate atmospheric model. In practice the attenuation is measured through room experiments, propagation measurements along the line-of-sight path [e.g. 4] or by extinction measurements of extraterrestrial sources such as the sun. [e.g. 5, 6, and 7]. Theoretical calculation and empirical determination of the millimeter wave emission of the atmosphere have been published by various workers. [8, 9, and 10]

Barrett et al. [8] have measured the atmospheric emission at

two zenith distances (60° and 70°) and at three frequencies (± 20, ± 60, and ± 200 MHz) centered on the $N=9^{+}$ resonance line of molecular oxygen at 61.151 GHz by their balloon flights, in which they found that for the 60- and 200-MHz channels the line widths as observed in those flights showed disagreement with the theoretically predicted values, which they attributed to the use of smaller line-width parameter $\Delta\nu$ in the Van Vleck-Weisskopf theory. They inferred that the discrepancy might be due to the assumption of Van Vleck and Weisskopf that the absorption coefficient due to many overlapping lines is merely the sum of the absorption coefficients of the individual lines. While at their 20-MHz channel even a larger line-width parameter than that actually used would not predict the observed values. In their theory they included two assumptions: first, the 5-mm wavelength radiation incident on the top of the atmosphere was assumed to be zero; second, the use of the Rayleigh-Jeans approximation to the Plank radiation law. However, the errors introduced due to the assumptions being small as compared with other uncertainties, they excluded the effect from the explanation of the discrepancy.

Meeks and Lilley [9] have calculated the opacity and the thermal emission of oxygen molecule in the earth's atmosphere. They suggested that the information about the vertical thermal structure of the atmosphere would be attainable from the satellite observation of the microwave brightness temperature as a function of the frequency around 60GHz, and that the relationship between the emission spectrum and the temperature as a function of height demonstrates that the emission at a given frequency repressents the average temperature in a layer of air roughly 10km deep.

Meeks [10] has calculated the emission and opacity of

the earth's atmosphere in the wavelength region from 7.5 to 3.7 mm. His result shows an excellent agreement with measured values of opacity at 6 and 4.3 mm wavelengths.

Barrett and Chung [11] have shown that from their theoretical analysis of the water vapor resonance line at 13.5 mm wavelength the data on the physical structure of the atmosphere would be obtained by the ground-based microwave observations.

While Croom [12] has calculated the atmospheric temperature at 13.5 and 1.64 mm water vapor resonance lines as observed from an earth satellite and obtained the result showing that the enhancement of the temperature at the resonance center of the 13.5 mm line would be 5°K even over the most favorable earth's surface (water), which is hard to be observed by the ground-based receiver.

The theoretical and empirical treatments of the atmospheric opacity and emission thus far cited have been performed in most cases by using the ARDC model atmosphere. [13] The model being such that its use would not deal with time-dependent phenomena such as diurnal and seasonal variations of the atmospheric opacity or emission.

Behaviors of water vapor distribution in the troposphere and the solar control of the atmospheric constituents variable in correspondence with solar zenith distance may give rise to profound effects in some cases on astronomical observations.

In this paper diurnal variation in sky emission temperatures at millimeter wavelengths in parallel with the measurements of the zenith emission at wavelengths of 8.6 and 3.2 mm are presented.

2. Observation

For the purpose of measuring the linear polarization of the Crab nebula at millimeter wavelengths, observations of the nebula were conducted during the period August-September 1968 using The University of Texas 16-foot diameter radio telescope at wavelengths of 8.6 and 3.2 mm. This telescope is described in references 14 and 15. The block diagram of the receiver is shown in Fig. 1.

The deflections in the record due to the nebula were seen over the tilting background. The background was found ascending for several pre-dawn hours and reaching a flat maximum at about an hour before sunrise, and thereafter descending rather rapidly than before. These variations in the background radiation were used to be found in every clear morning but barely found when humidity was very high. No drastic change in the background radiation due to ground sunrise was found.

For the purpose of confirming the characteristic variations of the background radiation, emission temperature at the zenith was measured at 8.6 and 3.2 mm wavelengths for several pre-sun-rise hours and approximately one post-sunrise hour for a period of about two weeks in late September and early October.

In the observations of the Crab nebula an integration time of approximately 200 seconds was applied in order to inprove the effective noise figure of the receiver and smooth out the effect of short period non-stationary atmospheric fluctuations since the antenna temperature due to the nebula was expected to be less than one degree Kelvin. Thus the minimum detectable temperature of the receivers used in the observations was approximately 0.5° K for the 3.2 mm wavelength radiometer and approximately 0.05°K for the 8.6 mm wavelength

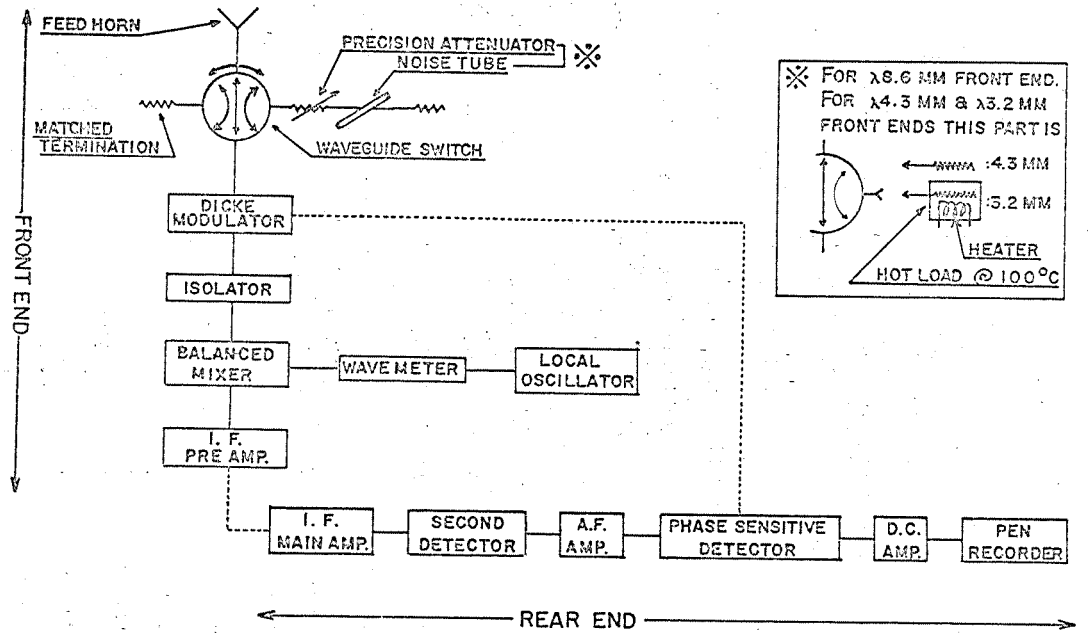

Fig.1. Block diagram of the receiver.

radiometer. This setup of the receivers enabled us to detect even slightest variations in antenna temperature.

After corroborative observations of the sky emission variations at the two wavelengths it was found that the emission temperature at the zenith showed, as was expected, regular variations with regard to the solar zenith distance at both wavelengths, that is, the sky emission temperature increased gradually and almost monotonously throughout early morning hours until it attained a short period (say, for 10 minutes or so) flat maximum at around an hour before ground sunrise and the temperature decreased rapidly thenceforth which kept up for hours.

Quantitatively describing these variations, on a clearest day the increase in antenna temperature at the 8.6 mm wavelength was very roughly $0.5^{\circ}K$ per hour and the rate of decrease after the peak was approximately $2^{\circ}K$ per hour. While at the 3.2 mm wavelength the temperature increase was found to be somewhat more gradual than in the case at the 8.6 mm wavelength, and its rate was estimated to be slightly less than 0.5° an hour. The rate of decrease at the 3.2 mm wavelength was found somewhat higher than at the 8.6 mm wavelength and was estimated to be 2 to $3^{\circ}K$ an hour. (vid. Fig.2). The onset of the decreasing phase was likely to have wavelength

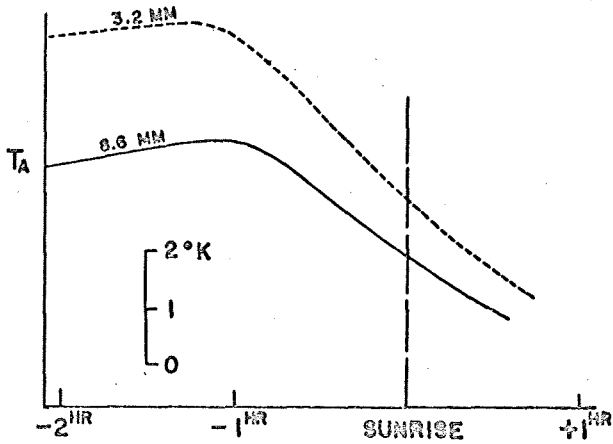

Fig.2. Observed antenna temperature variations with time.

dependence, that is, the 3.2 mm wave set in to decrease a little earlier than the 8.6 mm wave.

Calibration of the receiver was carried out by means of a matched termination at various temperatures. In the 8.6 mm radiometer a precision attenuator and an argon tube noise source were available. The precision attenuator readings were calibrated through the above procedure to enable to read approximately 2°C temperature difference. While, in the 3.2 mm wavelength radiometer, in which no precision attenuator was available, the calibration was performed directly with the matched termination, which was a very painstaking procedure to perform frequently. Hence, the evaluation of the antenna temperature due to the varying emission temperature was liable to be uncertain due to the delicate and awkward procedures in calibration.

The appearance of the maximum antenna temperature was clearly time-dependent with regard to the local ground sunrise, and hence the regular variations in antenna temperature was believed unquestionably to be due to some unknown source in sky.

However, for fear of possibilities of mistaking spurious antenna temperature variations due to instrumental and meteorological fluctuations for the intrinsic sky emission variations, due considerations were paid to discriminate what's what.

3. Possible mechanisms for the emission variations

At the first stage of this section the environments of the measurements at the time of the observations are introduced.

The possibility that the atmospheric temperature and humidity variations at the observing site might be the cause of the variations in the antenna temperature was feared at first. In order to investigate the possibility, the ambient temperature and the relative humidity near the antenna were monitored throughout respective observations, which remained on most days almost unchanged until about half an hour after sunrise. Accordingly, the variations in the antenna temperature were unmistakably not due to the variations in meteorological conditions at the ground level. Atmospheric pressure was not monitored but it may be inferable to have been stable at around 800 mb since the measured temperature and humidity remained almost constant.

Throughout observations the antenna was kept steady towards the zenith, and hence possible variation in ground radiation picked up by the antenna due to its varying posture was avoided. This warranted to eliminate the variations in the stray radiation of the ground as a possible source of the antenna temperature variations.

The receiver front end just behind the prime focus of the antenna consists of a cylinder in which all the waveguide components, a local oscillator, and an I.F. preamplifier are installed. Temperature inside the cylinder would come to saturation due to heat radiated by the local oscillator and the I.F. preamplifier after an hour's warming up. Thus, the thermally saturated front end would not exert any effect upon the output of the receiver.

The atmospheric and instrumental situations as stated thus far as well as the fact that the phenomena in the present discussion were clearly time-dependent with regard to the

solar zenith distance naturally led us to believe that the emission variations should be intrinsic variations possibly related with thermal and/or chemical properties of the atmosphere.

At the time of the observations the antenna beam was traversed by the Galaxy between right ascensions of around 4.5 and 6 hrs, however, the contribution of the galactic emission to the sky emission temperature at the wavelengths used should be essentially negligible except the constant 3°K cosmic background radiation omnipresent in space, and no distinct correspondence between the transit of the Galaxy and the timevarying sky emission was seen. Hence the contribution of the galactic radiation to the sky emission variations can be reasonably neglected.

Now it has become clear that the regularly varying sky emission is originated at some height in the earth's atmosphere between the F ionospheric layer and the troposphere.

Thermal and chemical properties of the earth's atmosphere are principally controlled by solar radiation and galactic cosmic rays through various processes such as heating, ionization, and dissociation of the atmospheric constituents. These processes occurring in various height ranges will be discussed in the following in relation to the time-dependent variations in the millimeter wave sky emission.

At first the contribution of the F_2-region to the sky emission variations is considered.

The F_2-region separated the shadowed portion and the sunlit portion of the atmosphere at about an hour before ground-sunrise. The sunlit portion of the ionosphere changes its conditions greatly, that is, electron concentration and

its temperature there set out to restore the daytime condition due to heating, ionization, dissociation, &c. of the constituent particles by solar X- and UV-radiations. Thus, the layer sunrise at the F_2-region distinctly separates the daytine and nighttime conditions in the layer sharply. Hence, the application of thermal radiation to the F_2-region seems to be worthwhile to be considered in relation to the periodic variations in sky emission temperature.

In this investigation validity of the Kirchhoff's law and local thermodynamic equilibrium are tentatively assumed. Actually, in the layers above the transition layers Kirchhoff's law would not hold any longer and also deviation from thermodynamic equilibrium may be great. However, since in the present case we are dealing with only a rough estimation of thermal emission in the F_2-region, even these assumptions would suffice the present requisite in investigating whether the F_2 acts as the source for the regularly varying temperature.

With these basic assumptions several equations are introduced for the purpose of calculating the thermal emission and absorption in the F_2-region.

The emissivity E of the thermal emitter per unit solid angle is expressed as follows: [16]

$$4\pi E = N_i N_e \frac{32\sqrt{2\pi}\, e^6 Z^2}{3c^3 m^{3/2} (kT)^{1/2}} \ln \frac{kT}{1.44\, Z\, e^2 N_i^{1/3}} \qquad (1)$$

The absorption coefficient r is obtained with Kirchhoff's law, $E_\lambda = r_\lambda B(T)$. In the radio frequency range the Rayleigh-Jeans approximation may be used with small error even at 95 GHz, then B(T) can be written as

$$B(T) = \frac{2kT}{c^2} f^2, \qquad (2)$$

where $f = c/\lambda$.

Under thermodynamic equilibrium the absorption coefficient is

$$\gamma_\lambda = E_\lambda \cdot \lambda^2 (2kT)^{-1}. \qquad (3)$$

Combining equations 1, 2, and 3, the absorption coefficient γ_λ is expressed as

$$\gamma_\lambda = N_i N_e \frac{4\sqrt{2\pi}\ e^6 Z^2 \lambda^2}{3\pi c^3 (mkT)^{3/2}} \ln \frac{kT}{1.44\ Z\ e^2 N_i^{1/3}} \qquad (4)$$

in which N_i and N_e represent number density of ion and electron, respectively. e and Z are electron and nuclear charge, respectively. c is the velocity of light, m electron mass, K Boltzmann constant, T kinetic temperature in ^oK, f wave frequency in Hz, and λ wavelength in cm.

As is immediately seen from Eq.4 the absorption coefficient is proportional to wavelength squared. Hence, it is intuitively expected that the absorption and hence the emission may take negligibly small values at millimeter wavelengths. In order to confirm this situation by means of Eq.4, typical values of N_i, N_e, and T for the daytime equilibrium in the F_2-region are taken to be $N_i \approx N_e \approx 5 \times 10^5 cm^{-3}$ and $T = 1500^oK$. Nuclear charge Z is taken to be 8 since most of ions in the F_2 consist of oxygen ions. With these values and from Equ.4 the

brightness temperature of the F_2-region thermal emission in the millimeter wave range was calculated to be vanishingly low.

Nighttime value of T at the F_2 heights is lower than the daytime value by a factor of one half to one third and nighttime N_e is lower by a factor of nearly two orders than the daytime value and hence the brightness temperature there is again negligibly small. Thus the F_2-region contribution to the millimeter wave emission may be safely ruled out from consideration.

In the F_1-region the situation is almost the same as in the F_2 and thus the contribution of the F_1-region to the millimeter wave emission is excluded likewise.

At the D-and E-region heights the time constants of ionization and recombination are of the orders of hours, days or even months according to the heights in those layers in which these reactions take place. Therefore, the emission due to ion-electron interaction and the emission due to molecular oxygen would show no such relatively short period variations as are needed in the present investigation.

So far we have seeked for the possible source of the regularly varying millimeter wave emissions in the F_2-layer down to the D-layer heights in vain, though these layers thus far investigated will reappear in the later stage as possible media which refract or scatter solar radiation downwards.

From above discussions it is now inferred that the source of the regularly varying millimeter wave emission lies at some height in the stratosphere or the troposphere in which molecular oxygen and water vapor concentrations are high.

Ionization in the lower atmosphere is caused chiefly by

the galactic cosmic radiation except the lowest kilometer over the ground in which ionization of air is chiefly due to radioactive matter in the soil. As is known, however, the intensity of the galactic cosmic radiation is low and show a very small diurnal variation of 0.1 to 0.2 % with a maximum at around local noon. Hence, the weak galactic cosmic radiation will not lend support to the interpretation of the regularly varying microwave emission in the present discussion.

Let us now consider another possible mechanism that may give rise to the phenomena, which seems to be the most effective factor in controlling temperature, O_2 and H_2O concentrations and hence millimeter wave emission at stratospheric and tropospheric heights before sunrise.

A portion of sun's radiant energy reaches stratospheric and tropospheric heights straying away by scattering and refraction from the direct beam toward F_2 heights in the course of its traveling in the atmosphere. Thus, the solar radiation straying into the lower atmosphere from the direct beam controls the atmospheric situation in the stratosphere and the higher half of the troposphere and hence the millimeter wave emission at those heights.

As is known, however, solar ultraviolet radiation is deeply absorbed in the higher atmosphere, and hence the radiation below $\lambda = 3200$A is cut off before it arrives at the troposphere. While at wavelengths greater than the visible range the absorption spectrum is due chiefly to the minor constituents in the atmosphere such as carbon dioxide and water vapor. Thus the infrared and visible parts of solar radiation refracted or scattered downwards can penetrate deep into the troposphere to heat and ionize the air at those heights.

Thus, it may be suggested that the downward bent solar radiation plays a leading role in controlling the situation in the millimeter wave emitting region in the decreasing phase of the sky emissions.

For convenience of description we will devide the day into five phases in accordance with the sequence of the emission variations.

PHASE I as we denote is the phase which starts at about an hour before ground sunrise and separates the nighttime and the daytime conditions.

PHASE II_α is the phase in which the atmospheric absorption and emission decrease constantly. This phase starts about an hour after ground sunrise (observationally the change in the decreasing rate of the sky emission would show a dull turning point at around several tens minutes after sunrise), and ends at around 14 hours in local time. PHASE II_α is immediately followed by PHASE II_β in which the sky emission increases gradually due to the heat loss of thé atmosphere. PHASE III follows PHASE II_β immediately. This phase is an inversion of PHASE I and may last for an hour or so.

PHASE IV is the final phase of the day and corresponds to the nighttime emission increasing phase which endures for nearly 10 hrs until the sky emission attains a pre-dawn maximum.

The sequence of the phases is illustrated in Fig.3 with temperature in the ordinate.

The nature of PHASE I has been discussed so far. It is a period in which the nighttime atmospheric condition is rapidly destroyed. This destruction is, as has been discussed already, due to the heating and the reduction of oxygen

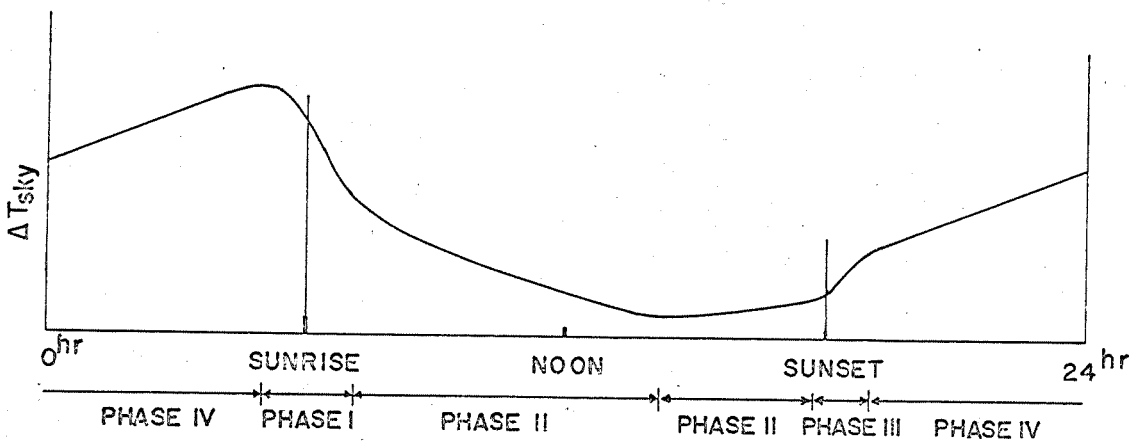

Fig.3. Assumed diurnal variation in sky emission temperature.

molecule and water vapor at heights around the upper troposphere due to the straying radiation from the direct solar beam illuminating the higher atmosphere. The straying light is the visible and infrared ranges of solar radiation since UV is strongly absorbed in the top layer of the ozonosphere as was stated before.

As the sun climbs the layer illuminated by the direct beam comes lower and lower, ionization and dissociation progress, and the temperature comes higher. In parallel with other changes due to the destruction of nighttime conditions in PHASE IV, the solar control of the atmosphere would bring the millimeter wave emission lower and lower for a couple of hours.

PHASE I is likely to be the most complex period of the day in which the rise and fall of atmospheric conditions take place concurrently.

In PHASE II solar radiation heats the atmosphere directly, and the march of this heating keeps up until sunset. Hence the sky emission temperature is naturally low. However, the atmospheric temperature comes to its saturation a couple hours after the meridian transit of the sun and thenceforth it decreases, and, therefore, before the time of the maximum atmospheric temperature the sky emission or opacity decrease gradually and after the atmospheric temperature has attained its peak the sky emission increases gradually as the sun goes down. Accordingly, it seems appropriate to make two subdivisions of PHASE II, that is, PHASE II_α which is given place to the period before the maximum atmospheric temperature, and PHASE II_β for the period after that.

At around sunset the heating of the atmosphere ceases

rapidly, cooling starts, and thus PHASE III sets in. As was stated, this phase is the inverse of PHASE I and therefore the processes taking place in PHASE I would occur in the reverse order in PHASE III. PHASE III may continue for some time, say an hour or so, and is immediately followed by PHASE IV.

PHASE IV endures throughout the night. In this phase the emission temperature of sky increases continuously until an hour before sunrise. At the peak of the emission temperature PHASE IV is taken over by PHASE I at which the day starts again.

The mechanism of the emission temperature increase in PHASE IV may be a concurrence of several processes taking place in regions from the ozonosphere down to the ground. These processes are:

a) Heat loss of the atmosphere after sunset.
   After ceasing of solar heating of the atmosphere the troposphere loses heat gradually bringing the atmospheric emissivity higher.

b) Gradual cooling of the ground.
   The heat emission of the ground attenuates gradually reducing the heating of the atmosphere through night. This brings the atmospheric emission higher.

c) Ozone heat loss.
   The atmospheric ozone near the region of 50km acts as an enormous heat reservoir absorbing solar radiation in Hartley absorption bands (2100-3000A) in the daytime. The stored energy by ozone released through long wave (infrared) radiation all through night impedes the cooling of the atmosphere, but as the stored energy is wasted this propping up of the atmospheric temperature

gets weaker resulting in a gradual cooling of the atmosphere. Thus, the atmospheric emission increases gradually.

d) Lowering of the height of zero water vapor concentration.

F. Shimabukuro [5] has reported that for the same value of pricipitable water the atmospheric attenuation is higher when the vertical distribution of water vapor concentrates lower in the atmosphere. This situation may have occurred as the air became cooler during the measurements. The height at which water vapor density becomes practically negligible comes lower (vid. Fig.4) throughout the night resulting in the increasing opacity or emission in the middle troposphere.

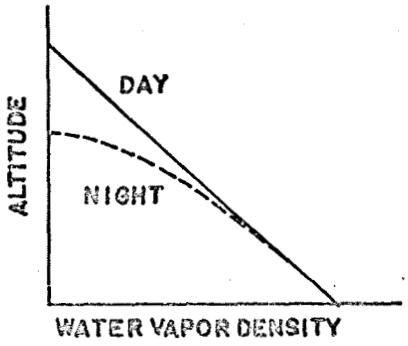

Fig.4. Height change of zero water vapor level between day and night.

e) Local atmospheric circulation.

The so-called mountain wind which occurs at summer nights is a circulation of air along mountainsides. (vid. Fig.5). This circulation may act as a carrier of cool and humid air in the surrounding valleys to the over-summit region. Thus, a constant flow of cool and humid air from the region over the top of the mountain fills the antenna beam pointing at the zenith to increase the antenna temperature. The mountain wind sets in at around midnight and reaches a peak sometime before

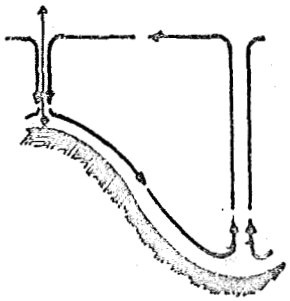
Fig.5. Mountain-valley air circulation at night (mountain wind)

sunrise. The atmospheric condition favorable to the occurrence of this air circulation is limited to only a windless night, and when mixing of air prevails there is no such circulation. The atmospheric circulation, when occurred under a favorable meteorological condition, may have contributed to the time variations in the opacity and emission of the atmosphere at the zenith over the observer since The University of Texas 16-foot diameter radio telescope used in the observation is situated close to the top of Mt. Locke. (For the atmospheric circulation vs. sky emission temperature, see pp.29 - 33 in this issue).

The preocesses a through d and possibly e which keep their march throughout the night come to their termination concurrently at some time before sunrise and are taken over by the solar control of the atmosphere in PHASE I.

The occurrences in PHASE I through PHASE IV are summarized in Table I.

It is naturally inferred that in the observations of weak extraterrestrial radio sources in the microwave range the relation between the antenna temperature due to a source and the zenith distance of the source would show specific traits in accordance with the respective phases.

Let the atmospheric opacity be τ_1 and τ_2 for the observations before and after the meridian transit of the source, respectively. Then, $\tau_1 > \tau_2$ in PHASE I, $\tau_1 > \tau_2$ in PHASE IIα, $\tau_1 < \tau_2$ in PHASE IIβ, $\tau_1 < \tau_2$ in PHASE III, and $\tau_1 < \tau_2$ in PHASE IV. In PHASE I and PHASE III the atmospheric opacity and hence emission vary irregularly, and accordingly the curve for antenna temperature vs. zenith distance would show irregularities in

Table I

PHASE	Phenomena	Cause
I*	Onset of decrease in sky emission at about one hour before sunrise. Transient period between night and day.	Onset of solar control of lower atmosphere due to downward scattering of solar radiation and decay of nighttime atmospheric conditions.
IIα	Continuous decrease of sky emission.	Gradual heating of air by direct solar radiation.
IIβ	Gradual increase of sky emission.	Gradual cooling of air a few hours after meridian transit of sun.
III*	Increase of sky emission at around sunset. Transient period between day and night.	Ceasing of solar heating of lower atmosphere. Reverse processes of PHASE I.
IV	Continuous increase of sky emission.	Heat loss of atmosphere. Concurrence of several processes.

* May have wavelength dependence in the onset time.

accordance with the varying opacity. In particular when an observation is made in the period extending over PHASE IV and PHASE I, PHASE II and PHASE III, PHASE III and PHASE IV, and possibly PHASE II_α and PHASE II_β, the plot of antenna temperature vs. zenith distance would be complicated. These situations are illustrated in Figs.6(a) through (e) and Figs.7(a) through (c).

As are readily seen in these figures, the plots of antenna temperature vs. zenith distance obtained in the observations made in PHASE I, PHASE III, and the interphase periods do not show a simple curve as appears in PHASE II and PHASE IV. In these cases the exact brightness temperature of the source may not be determined so simply as in the case that the atmospheric attenuation is linearly changing.

At millimeter wavelengths at which atmospheric absorption is considerably high, the brightness temperature of an extraterrestrial radio source can be determined by extending the plot of the antenna temperature vs.

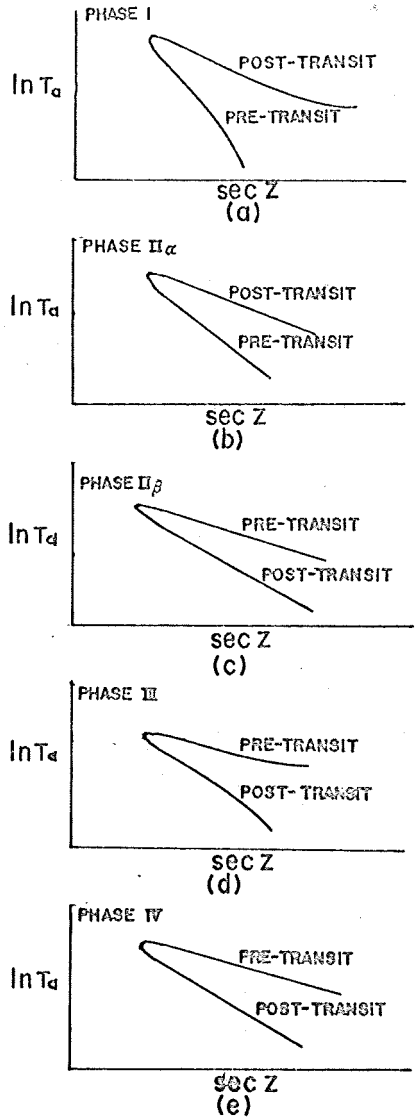

Fig.6. Expected $\ln T_a$ vs. sec Z curves for respective phases.

sec Z curve to sec Z=0 when the atmospheric attenuation is not changing during the observation, and the intercept at secZ=0 gives the brightness temperature of the source. If the attenuation changes at a constant rate r, the plot of the pre- and post-transit $\ln T_a$ vs. sec Z values will give a regression curve. Then the brightness temperature of the source is determined by extending the inner bisector of the regression curve to sec Z=0. This situation is illustrated in Fig.8. In this figure intercepts a and c, which give brightness temperature for, say, pre- and post-transit measurements, represent false values. The true brightness temperature is found at b which is the intercept of the bisector of the plots for the pre- and post-transit measurements. Accordingly, if the plot of the measured $\ln T_a$ vs. sec Z values gives a sinuous regression curve as appearing in Figs. 6 and 7, there is no way to

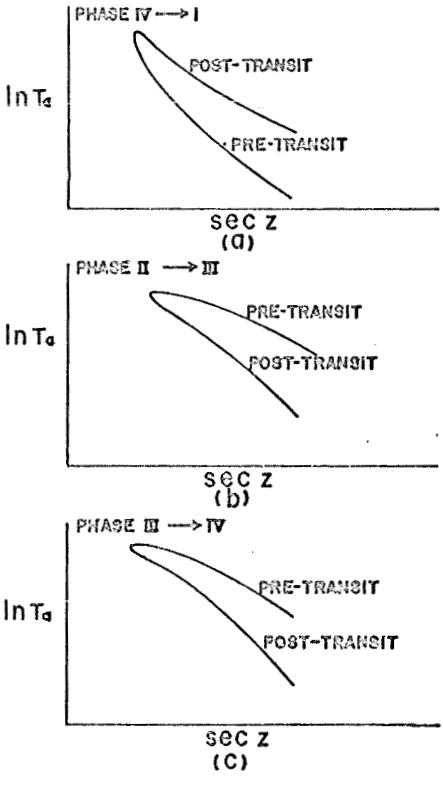

Fig.7. Expected interphase $\ln T_a$ vs. secZ curves for pre- and post-transit measurements of a source.

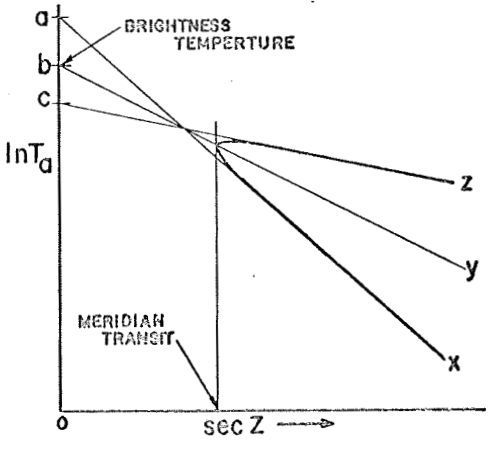

Fig.8. $\ln T_a$ vs. sec Z under linearly varying attenuation.

find out the true brightness temperature of the source. Therefore, observation of weak sources should be made either in PHASE IV or in PHASE II.

4. Wavelength dependence of the diurnal variations

As was stated in section 2, the onset of PHASE I at the 8.6 and 3.2 mm wavelengths are slightly different, that is, the onset of PHASE I at the 8.6 mm wavelength retards slightly compared with that at the 3.2 mm wavelength. This may be interpreted by the difference in the attenuation at the two wavelengths. The 3.2 mm wave is more sensitive than the 8.6 mm wave to the variations in attenuation due to varying atmospheric conditions described previously. (vid. Fig.9). From above statement, it may be inferred that in PHASE III the rise of sky emission at the 3.2 mm wavelength should be steeper than in the case at the 8.6 mm wavelength and the temperature increase at the 3.2 mm wavelength in this phase should be greater than at the 8.6 mm wavelength.

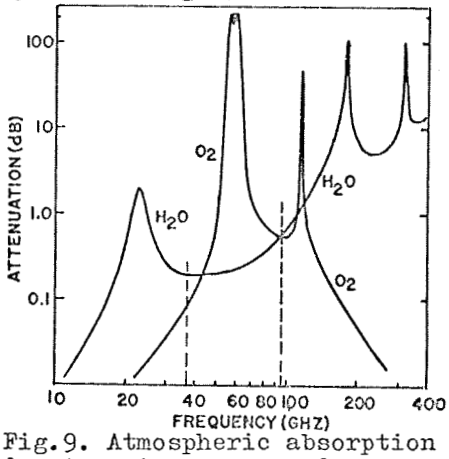

Fig.9. Atmospheric absorption due to water vapor and oxygen molecule.

5. Seasonal variations

The ratio of the antenna temperature to brightness temperature of a source is dependent upon the season in which the observation is made. The ratios for some planets at various millimeter wavelengths have been reported by Tolbert et al. [14] for the period July-November 1964. Their results are shown in

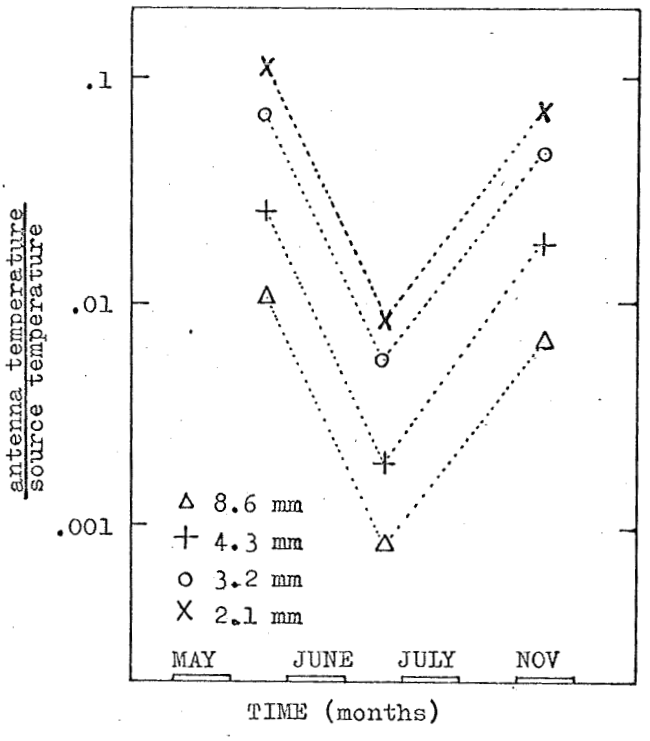

Fig.10. Variations in the ratio antenna temperature/brightness temperature of some planets during calender 1964. After Tolbert et al.

Fig.10. The variations seen in the figure are unmistakably due to the change in humidity in the atmosphere. The minimum T_a/T_s ratios for all the wavelengths come, as are readily seen in the figure, in midsummer in which humidity is the highest in the year. From the results of Tolbert et al. it is naturally inferred that seasonal variations should exist in the sky emission and opacity which are dependent upon the wavelength used in the observation.

6. Discussion and conclusion

In the latter part of September, repair work of the astrodome started, and the operation hour of the telescope was limited to nighttime only. Therefore, the observation did not cover the whole process of the sky emission variations. Accordingly, the present discussions are based on a short time observation of the daylong variations which covered only several hours

from midnight through about an hour after sunrise. Therefore, PHASE II, PHASE III, and the first half of PHASE IV have no experimental bases. Hence, we had to speculate about the rest of the phases from the observations made in PHASE IV and PHASE I in order to construct the diurnal variation curve of the sky emission as shown in Fig. 3.

However, it may be stated that the periodic and recurrent variations in sky emission and opacity exist besides the large scale variations due to non-periodic changes in meteorological conditions.

These regular variations may have a temperature amplitude of , say, 10°at the most as observed at the height of as high as 2000 meters. This amplitude would be much smaller for an observer near see level. Therefore, in the observation of strong radio sources such as the sun, this small amplitude variations in the attenuation would naturally be passed over without being noticed. However, observations of weak radio sources in which the antenna temperatures due to those sources are less than the amplitude of the temperature variations of sky may suffer from the varying opacity and emission even though the weather is ideally fine and irregular variations in the atmosphere should be completely negligible. Therefore, it may be said that in order to determine the exact value of brightness temperature of a weak source, as was mentioned already, observation should be made during PHASE II or PHASE IV in which the decrease or increase of the atmospheric attenuation are relatively constant aside from the effect of non-periodic variations in meteorological conditions.

There remain some questions about the nature of the phenomena: They might be localized phenomena, may have relations

with the solar cycle and activities, and so forth. However, since the observations were carried out in a limited period, there is no means to answer these questions. Solution of these questions calls for the observations of the phenomena at various locations and at a variety of wavelengths covering 24 hours of the day and extending over a long space of time. In PHASE II_α and II_β the observations of the phenomena may be difficult due to solar radiation straying into the antenna through its sidelobes. Even if the sidelobe level of an antenna is 30 dB lower than that of its main lobe, the spurious response due to the straying solar radiation would come up to several degrees which is almost comparable to the amplitude of the sky temperature variations in the present discussions.

The two wavelengths of 8.6 and 3.2 mm used in the observations are both in the radio windows between the molecular oxygen and water vapor resonance lines at 13.5, 5, and 2.35 mm. Observations of the phenomena at or near these resonance lines will reveal which makes more contribution to the generation of the phenomena, water vapor or oxygen molecule; and will give more precise information for the interpretation of the wavelength dependence of the onset of PHASE I and PHASE III, and possibly about the height of the source for the phenomena. They will also give some information about the physical and chemical properties of the lower atmosphere, possibly including the stratosphere, as a supplementary means for the calculations and experiments of various workers cited in section 1 in this paper.

In closing, need of long-term observations of the sky temperature is emphasized in order to enable meteorologists to acquire further knowledge about the troposphere and pos-

sibly the stratosphere, and to enable astronomers to know the behavior of the atmospheric absorption of microwaves the knowledge of which is a prerequisite for the determination of exact brightness temperature of extraterrestrial radio sources.

References

1. J. H. Van Vleck and V. F. Weisskopf, " On the shape of collision-broadened lines," Rev. Mod. Phys., 17, April-July 1945.
2. J. H. Van Vleck, " The absorption of microwaves by oxygen," Phys. Rev., 71, No.7, April 1947.
3. J. H. Van Vleck, "The absorption of microwaves by uncondensed water vapor," Phys. Rev. 71, No.7, April 1947.
4. A. W. Straiton and C. W. Tolbert," Anomalies in the absorption of radio waves by atmospheric gasses," Proc. IRE, 48, No.5, May 1960.
5. R. J. Coates, " Measurements of solar radiation and atmospheric attenuation at 4.3-millimeters wavelength," Proc. IRE, 46, January 1958.
6. F. I. Shimabukuro," Propagation through the atmosphere at a wavelength of 3.3 mm," IEEE Trans. Antennas and Propagation," AP-14, No.2, March 1966.
7. A. Tsuchiya and K. Nagane," Atmospheric absorption in microwave solar observation and solar flux measurements at 17 GHz," Publ. Astron. Soc. Japan, 17, 1965.
8. A. H. Barrett, J. W. Kuiper, and W. B. Renoir," Observations of microwave emission by molecular oxygen in the terrestrial atmosphere," J. Geophys. Res., 71, No.20, October 1966.
9. M. L. Meaks and A. E. Lilly," The microwave spectrum of oxygen in the earth's atmosphere," J. Geophys. Res., 68, No.6, 1963.
10. M. L. Meaks," Atmospheric emission and opacity at millimeter wavelengths due to oxygen," J. Geophys. Res., 66, No.11 November 1961.

11. A. H. Barrett and V. K. Chung," A method for the determination of high-altitude water-vapor abundance from groundbased microwave observations," J. Geophys. Res. 67, No.11, October 1962.
12. D. L. Croom," The possible detection of atmospheric water-vapor from a satellite by observations of 13.5 and 1.64 mm H_2O lines," J. Atmosph. Terr. Phys., 28, 1966.
13. U.S. Air Force, Handbook of Geophysics, revised ed. Macmillan Co., New York, 1960.
14. C. W. Tolbert, A. W. Straiton, and L. C. Krause, " A 16-foot diameter millimeter wavelength antanna system, its characteristics and its application," IEEE Trans. Antennas and Propagation, AP-13, No.2, March 1965.
15. J. R. Cogdell," Calibration program for the 16-foot antenna," NASA Tech. Rep., NGL-006-1, January 1969.
16. G. Elwert," Der Absorptionskoeffizient an langwellen Grenze des Kontinuierlichen Roentgen Spectrums," Z. Naturforsch. 3a, 477, 1948.

ANOMALOUS SKY TEMPERATURE VARIATION WITH ZENITH DISTANCE MEASURED ON A MOUNTAIN-TOP AT A CALM NIGHT AT A WAVELENGTH OF 3.2 MM

Observations of extraterrestrial radio sources in the microwave range sustain attenuation due to oxygen molecule and uncondensed water vapor in the atmosphere. In particular for waves at wavelengths shorter than about 20 mm, the atmospheric absorption is considerably high and around the resonance frequencies of molecular oxygen and water vapor its effect is profound. Hence a radio source moving in the sky gives a varying antenna temperature in accordance with the zenith distance of the source. This is described in the form

$$T_a = AT_s \exp(-\tau \sec Z) \qquad (1)$$

where T_a is the antenna temperature due to the source, A a constant of proportionality, T_s brightness temperature of the source, τ the opacity at the zenith, and Z zenith distance of the source.

The opacity τ can be determined by the aid of Van Vleck-Weisskopf equation [1, 2, and 3] and an appropriate atmospheric model. [e.g. 4]

Or conversely, τ may be obtained by applying the relation $\ln T_a$ vs. $\sec Z$ whose plot is a straight line with a slope equal to $-\tau$.

Without emitting source the atmosphere is not an absorbing matter any longer but acts as an emitter of waves itself. Then the antenna temperature due to the atmospheric emission is expressed as

$$T_a = T_{sky}(1 - e^{-\tau \sec Z}) \qquad (2)$$

in which T_{sky} is the average temperature of the atmosphere.

This situation is illustrated in Fig.1.

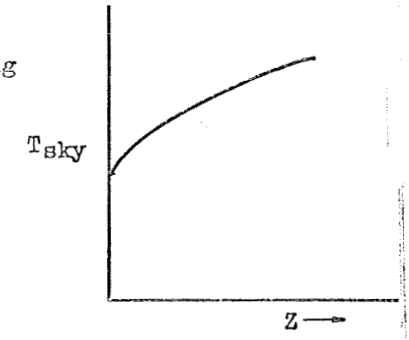

Fig.1. Normal T_{sky} vs. zenith distance.

For the purpose of confirming this relation by experiment, The University of Texas 16-foot diameter radio telescope installed near the top of Mt. Locke near Fort Davis, Texas was used at a wavelength of 3.2 mm. The measurement was conducted at several clear nights in September 1968. Since the wavelength used is in the radio window between the 5- and 2.53-mm resonance lines of molecular oxygen and since the absorption due to water vapor is not very high at this wavelength, the variation in sky emission due to increasing zenith distance was expected to be low. Therefore, a long integration time of approximately 100 seconds was applied in order to improve the effective sensitivity of the receiver. Thus, the minimum detectable temperature of the radiometer attained a value of about $2^{o}K$.

The measurement was carried out by tilting the antenna at intervals of 10 degrees from the zenith down to a zenith distance of 80 degrees. In order to separate the effect of the ground emission from the intrinsic sky emission variation with zenith distance, a check was made by tilting the antenna from the zenith toward south, east, and west. Northward tilting was not made since the sight in this direction was obstructed by the peak of Mt. Locke.

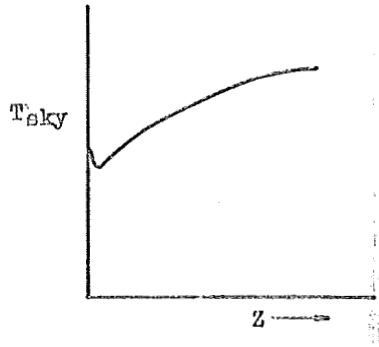

Fig.2. T_{sky} vs. zenith distance under anomalous zenith opacity as observed.

In the data thus taken an anomalous bulge of antenna temperature around the direction toward the zenith was found. A sketch of this abnormal temperature variation with zenith distance is shown in Fig.2. The feature of the temperature variation as seen in the figure is somewhat different from the curve shown in Fig.1. The minimum temperature was found unexpectedly at around 30 degrees from the zenith, and this anomaly was found at a calm night.

At calm nights in this season the anemoscope installed near the antenna site showed no definite direction which was the indication of the existence of turbulent vertical air motions along the mountainside.

As is well known there is a constant air flow along mountainsides: downward flow at night and upward flow in the daytime. The former is called mountain wind and the latter valley wind. These winds are generated through expansion or contraction of air as mountainsides warm up in the daytime or cool down in the nighttime, and they are known to be observed in summer. [5 and 6] Mountain wind sets in at around midnight and reaches its peak of development before sunrise. The downslope wind changes its direction near the bottom of the valley and blows upwards from there. The upward flow changes its direction at a certain height over the valley and soon changes its direction again towards the top of the mountain. Thus, the atmospheric circulation reccurs and keeps up for hours as the mountainsides cool down.

The mountain-valley circulation may play a role as a carrier of humid and cool air from the surrounding valleys to the over-the-mountaintop region. Thus, this circulation makes the overhead region of the observer filled with humid and cool air.

When the antenna beam traverses the flux of the circulation the antenna temperature due to the humid and cool air in the overhead region of the observer would show a higher value than that expected from the usual T_a vs. zenith distance relation. This is illustrated in Fig.3. As is shown in the figure, the direction of the antenna beam between Z_o and Z_1 is just in the flux of the downward air flow toward the observer at O, and in this range the antenna temperature would show a slightly higher value than it should be in the normal case, and the antenna temperature for beam direction lower than OZ_1 would obey the usual T_a vs. Z relation.

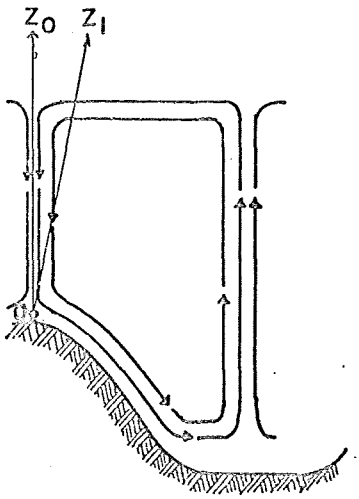

Fig.3. Air circulation due to mountain wind and antenna beam directions penetrating it.

The effect of the anomalous zenith opacity upon the antenna temperature due to a source passing the zenith region is shown in Fig.4.

When wind is strong enough, the circulation does not exist because of mixing, and then the antenna temperature would show no anomaly any longer and would obey the usual T_a vs. Z law.

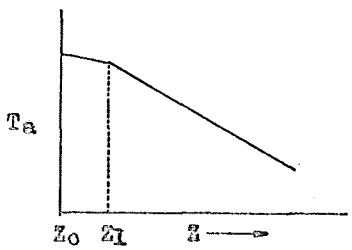

Fig.4. T_a vs. zenith distance for a source passing zenith with anomalous opacity due to mountain wind in the nighttime.

No measurement of the same kind was not made in the daytime since if the sun is above the horizon its contribution to the antenna temperature would not be negligible and would vary in accordance with the relative position

between the sun and the antenna. This varying contribution of the sun would confuse the measurement.

Since the period of observation was very short we could not take enough data for making rigorous discussions for the phenomenon. However, it may be suggested that the enhanced absorption or emission in the zenith region would give rise to an anomalous $\ln T_a$ vs. $\sec Z$ curve for a source passing through this region over the mountaintop as was stated already and shown in Fig.4.

Finally, emphasis is made that in selecting the antenna site for a radio telescope in the microwave range in which the effect of atmospheric absorption is considerably high, various investigations should precede about local atmospheric conditions which exert undesirable effects on astronomical observations, though the effect of the atmospheric circulation reported here would not be so annoying since their occurrence is fairly limited in direction, season, and weather.

References

1. J. H. Van Vlecke and V. F. Weisskopf, " On the shape of collision-broadened lines," Rev. Mod. Phys., 17, April-July 1945.
2. J. H. Van Vleck, " The absorption of microwave by oxygen," Phys. Rev., 71, No.7, April 1947.
3. J. H. Van Vleck, " The absorption of microwaves by uncondensed water vapor," Phys. Rev., 71, No.7, April 1947.
4. U.S.Air Force, Handbook of Heophysics, revised ed., Macmillan Co., New York, 1960.
5. A. Kh. Khrgian, Ocherki razvitiya meteorologii. Gidrometeoizdat, Leningrad, 1959.
6. P. N. Tverskoi, Physics of the atmosphere, English translation. Jerusalem, 1965.

MEASUREMENTS OF LINEAR POLARIZATION OF THE MOON AT MILLIMETER WAVELENGTHS

Abstract--Measurements of the linear polarization of lunar thermal radiation were carried out at wavelengths of 8.6, 4.3, and 3.2 mm using The University of Texas 16-foot diameter millimeter wavelength telescope in the period July-September 1968. At 8.6 mm wavelength it was found that the measured position of the maximum polarization removed towards the limb away from that expected from a smooth surface model. Assuming that this is due to the effect of surface roughness, the average slope of roughness is estimated to be $8^{\circ} \pm 2^{\circ}$. While at 4.3 mm wavelength fluctuations brought on by atmospheric variations have made the estimation of the polarization difficult, but the data shows a sign of polarization at this wavelength. Whereas, at 3.2 mm wavelength no definite sign of polarization was found. From the analyses of 10-odd clear nights' data it is inferred that the polarization should be very weak at 3.2 mm wavelength. From these results and Bastin's measurement of the polarization at a wavelength of 1.5 mm, the scale of surface roughness is inferred. It is indicated that the small scale roughness may be distributed around a radius size of 0.9 mm.

1. Introduction

Troitsky [1] has suggested the possibility that information about the surface roughness and the dielectric constant of the lunar surface might be obtained from the measurement of the linear polarization of the lunar thermal emission.

Assuming a smooth and homogeneous surface, power reflectivity R for a plane electromagnetic wave is expressed as the square of the Fresnel coefficient as

$$R_{\parallel} = \left| \frac{\varepsilon \cos\theta - \sqrt{\varepsilon - \sin^2\theta}}{\varepsilon \cos\theta + \sqrt{\varepsilon - \sin^2\theta}} \right|^2 \qquad (1)$$

for linear polarization with the electric vector parallel to the plane of incidence, and

$$R_{\perp} = \left| \frac{\cos\theta - \sqrt{\varepsilon - \sin^2\theta}}{\cos\theta + \sqrt{\varepsilon - \sin^2\theta}} \right|^2 \qquad (2)$$

for the orthogonal polarization.

Here θ is the angle of wave incidence and ε the dielectric constant of the surface material of the moon.

The emissivity $E_{(\theta)}$ for the thermal radiation emitted from a smooth surface in the direction θ is expressed by the Kirchhoff's law as

$$E_{\parallel} = 1 - R_{\parallel(\theta)} \qquad (3)$$

and

$$E_{\perp} = 1 - R_{\perp(\theta)} \qquad (4)$$

The brightness temperature distribution on the moon measured with an infinitely narrow antenna beam is given by

$$T_{D_0} = \left[E_{\parallel} \cos^2(D - D_0) + E_{\perp} \sin^2(D - D_0) \right] \cdot T \qquad (5)$$

and for the orthogonal polarization

$$T_{(D_0 + \pi/2)} = \left[E_{\parallel} \sin^2(D - D_0) + E_{\perp} \cos^2(D - D_0) \right] \cdot T \qquad (6)$$

in which D_0 is the angle between the lunar equator and the orientation of the antenna polarization; D is the radius on which the point of observation is situated.

Then the polarized component ΔT_p is obtained by taking the difference between T_{D_0} and $T_{(D_0+\pi/2)}$, i.e.,

$$\Delta T_p = T_{D_0} - T_{(D_0+\pi/2)} \tag{7}$$

After Troitsky's suggestion an appreciable amount of the results of measurements at various wavelengths have been reported. These measurements have furnished us with useful informations about the properties of the lunar surface together with the results obtained by radarmetric means.

Particularly, measurements of the polarization at millimeter wavelengths seem to be interesting because of their short wavelength with respect to the influence of surface roughness upon the waves. From this view point, observations of the polarization were conducted at wavelengths of 8.6, 4.3, and 3.2 mm using The University of Texas 16-foot diameter radio telescope in the period July-September 1968. The characeristics of the antenna are well described in Refs.2 and 3. The resolving power of the antenna is approximately 7' for λ8.6 mm, 3.5' for λ4.3 mm, and 2.8' for λ3.2 mm, respectively.

In the following are presented the results obtained in these measurements.

2. Observations and their results

As is well known, propagation of millimeter waves is subject to the influence of oxygen molecule and water vapor in the atmosphere. Hence, even when atmospheric condition is most favorable, the effect of small scale irregularities of the atmosphere inevitably deteriorates the data obtained particularly at the 4.3 and 3.2 mm wavelengths. Therefore, in the measurements of the polarization it is most desirable to

measure the ΔT_p directly. However, at the time when these observations were conducted the radiometers for the three wavelengths used were not equipped with such a device as to measure the ΔT_p directly. Hence, in order to obtain the ΔT_p with those radiometers we had to resort to a round-about method to measure T_{D_0} and $T_{(D_0+\pi/2)}$ in separate scans. For the purpose of securing the symmetry of the data for the two orthogonal polarizations, either T_{D_0} or $T_{(D_0+\pi/2)}$ was measured in pre-transit hours, and the rest in post-transit hours. At around the meridian transit of the moon the feed horn was rotated by 90° to change polarization. The data taken in pre- and post-transit hours were averaged separately, and then taking the difference of the two averaged curves ΔT_p was obtained finally.

The method adopted in the observations required a long span of time, during which atmospheric conditions often changed appreciably. Hence, at the 3.2 mm wavelength, as will be seen later, the effect of atmospheric variations was so severe that no definite sign of polarization could be found. Atmospheric scintillations exert a blurring effect on the edge of the moon's disk when the antenna beam transits there. This makes the size of the lunar disk vary from time to time, and hence makes difficult the processing of the data and the comparizon of the curves for the respective polarizations.

Measurements were centered in the detection of the polarization at 3.2 mm wavelength, and the other two wavelengths were adopted as sabsidiary means.

Measurements were carried out at the 8.6 mm wavelength at first. An example of the results of these measurements is shown in Fig.1. The curves shown in the figure were obtained by one scan for the respective polarization under a favorable weather

condition. The ΔT_p deduced from Fig.1 is shown in Fig.2 in which, as is readily seen, the position of the maximum ΔT_p as measured comes slightly outside the theoretically expected position.

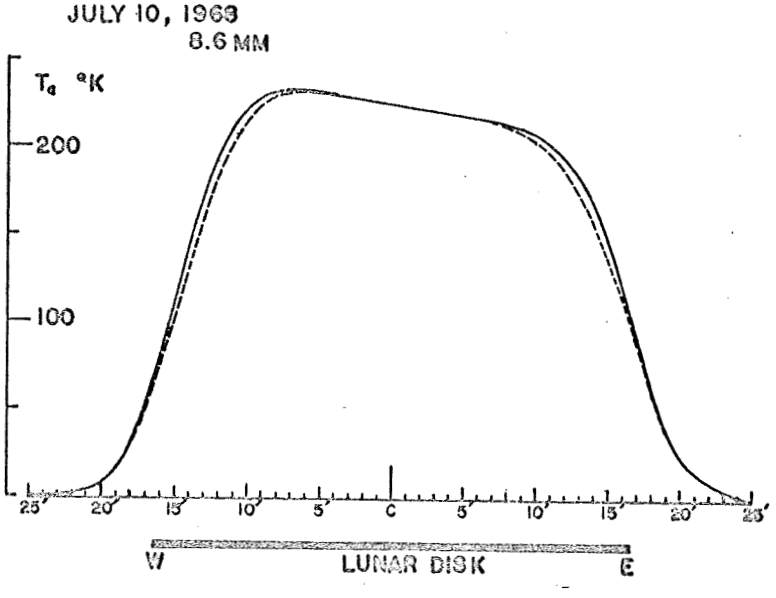

Fig.1. Measured antenna temperatures for horizontal (———) and vertical (------) polarizations at 8.6 mm wavelength.

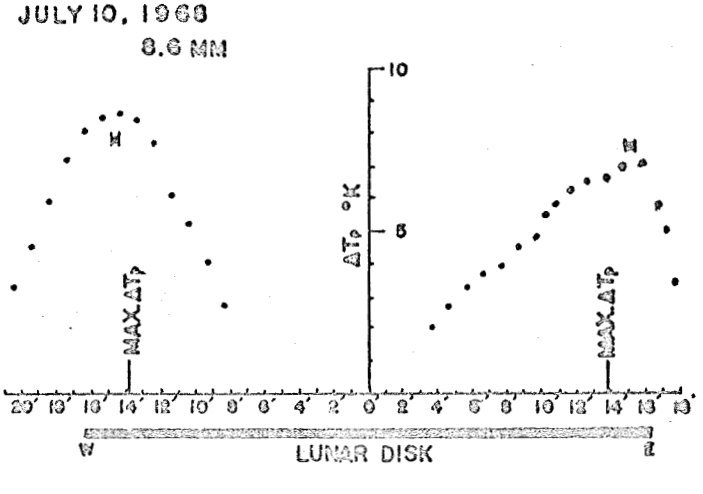

Fig.2. ΔT_p obtained from Fig.1. Attention to the difference between theoretical and measured positions of maximum ΔT_p.

Similar effect can also be found in the results obtained by Moran [4] at a wavelength of 8.6 mm.

Theoretically it is expected that the position of the maximum ΔT_p is situated at a point satisfying the following relation:

$$\theta \approx \cos^{-1}\sqrt{\varepsilon - 1}/4(\varepsilon - 1) \qquad (8)$$

in which θ is the angle of wave incidence and ε dielectric constant. Practically, however, the temperature distributions are measured with an antenna with a finite resolving power, and accordingly the angle θ comes at a slightly different position. The maximum ΔT_p appearing in Fig.2 was obtained by applying the effect of the antenna's smoothing effect on the theoretical ΔT_p distribution. The outward displacement of the maximum ΔT_p position may be explained by taking into consideration the effect of surface roughness which makes the angle of wave incidence at the point of observation smaller than it should be in the case of a smooth surface, that is, the slope of the undulations facing to the observer makes the normal at the point of observation tilt toward the observer. Thus, the angle between the propagation and the actual normal becomes smaller than in the case of a smooth surface. Thus, the lunar surface as observed appears rather flat than a sphere due to surface roughness. Then, at the point where the maximum ΔT_p should occur when the surface is completely smooth the angle θ which satisfies Eq.8 would not be attained. At this point the actual angle of incidence is θ minus average slope σ of undulations. Thus, the largest ΔT_p would naturally be found at a point which steps over the theoretically predicted position. This situation is illustrated in Figs.3 and 4. In Fig.3 is shown the effect of an undulation on the local normal.

The normal for the smooth surface $\overrightarrow{pn_o}$ tilts to $\overrightarrow{pn_{act.}}$ due to an undulation with its average tangent $\overrightarrow{ps}$ and average slope σ. Then the angle of tilt of normal $\overrightarrow{pn_o}$ to $\overrightarrow{pn_{act.}}$ is also σ. Hence, smooth surface angle θ reduces to rough surface angle θ'.

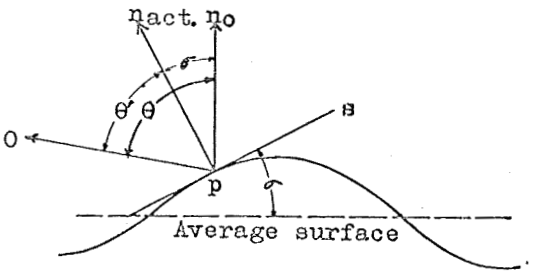

Fig.3. Effect of an undulation on surface normal. Average surface normal pn_o tilts to pn_{act} due to slope σ.

Fig.4 illustrates the effect of undulations somewhat more generally than in Fig.3. The maximum ΔT_p is expected to occur at distance R_1 from the disk center in the case of a smooth surface model. Observationally, however, it was found at R_2. At point p, which corresponds to distance R_1, the smooth surface normal $\overrightarrow{pn_1}$ tilts to the actual normal $\overrightarrow{pn_p}$ making angle θ reduce to angle θ_p. Thus, at point p the maximum ΔT_p condition would not be satisfied. Whereas, at point q, which corresponds to distance R_2 from the disk center, angle θ_2 for smooth surface reduces to $\angle 0_2 q n_q$ or $\emptyset$ due to slope σ to satisfy the maximum ΔT_p condition in Eq.8.

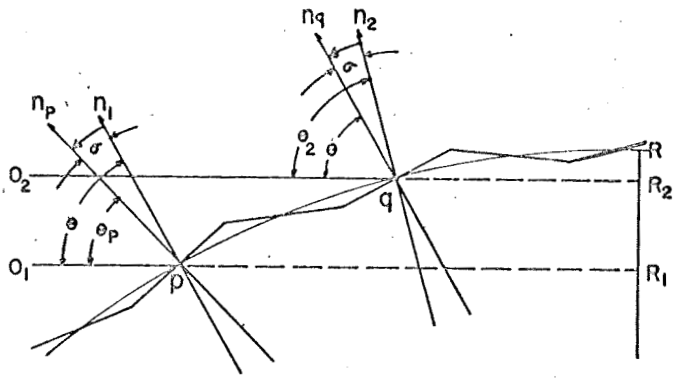

Fig.4. Effect of undulations to drive the maximum ΔT_p position outwards.

The preceding assumption lends support not only to the

explanation of the outward displacement of the maximum ΔT_p position but also to the investigation of the average slope of surface roughness whose method is selfexplanatory in the preceding assumption. Using the same symbols as appear in Fig.4 and the semidiameter R of the disk, the average slope σ is given by

$$\sigma = \theta_2 - \theta = \theta - \theta_p = \sin^{-1}(R_2/R) - \sin^{-1}(R_1/R) \qquad (9)$$

since $\theta = \sin^{-1}(R_1/R)$ and $\theta_2 = \sin^{-1}(R_2/R)$.

Thus, measurement of the linear polarization of the moon's thermal radiation enables one to determine the average slope of surface roughness. However, of course, the position at which the maximum ΔT_p occurs is dependent upon the dielectric constant of the surface material on the moon, and hence the average slope σ also depends upon the dielectric constant. Moran adopted a value of 1.6 for the dielectric constant, and in our case computations were carried out with the dielectric constant of 1.8. Naturally, the value of the average slope must be slightly different between that of Moran and that of ours. However, uncertainties associated with the measurements by means of the previously mentioned method may not be small, so that the difference ($< 1^\circ$ for all the possible values of dielectric constant of the lunar surface) due to the different dielectric constants may not matter in the present investigation since we are feeling that it should be improper to mention of the exact value of the average slope by using the data available to us now. Therefore, only a very rough estimation of the average slope as measured at the 8.6 mm wavelength will be given here. By the aid of Eq.9 the average slope is estimated to be $8^\circ \pm 2^\circ$ from the data obtained at this wavelength. From the data obtained by Moran [4] at 8.6 mm wavelength the slope is estimated to be nearly the same value, though his mod-

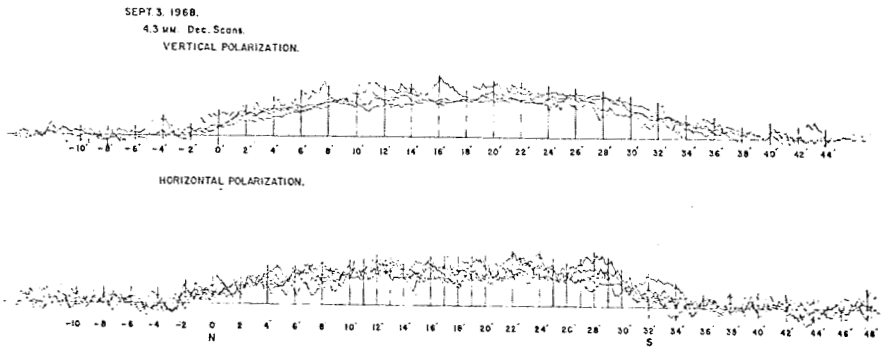

Fig.5. Scan curves for vertical (upper) and horizontal (lower) polarizations for 4.3 mm wavelength. Sept. 3, 1968.

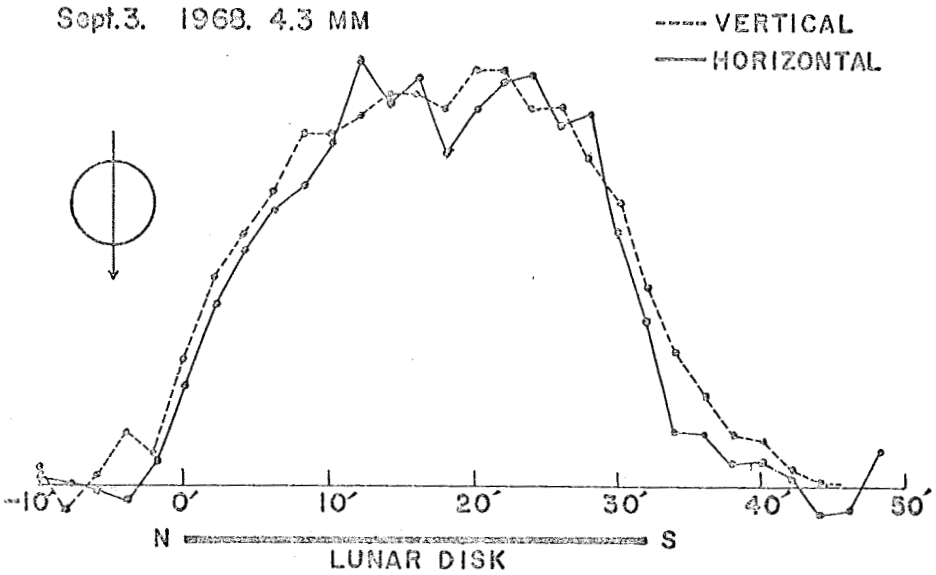

Fig.6. Averaged curves of Fig.5 for horizontal (———) and vertical (- - - - -) polarizations. Pay attention to the swell at 28' from the north limb in the curve for horizontal polarization. Except this point vertical polarization is seen at around limbs.

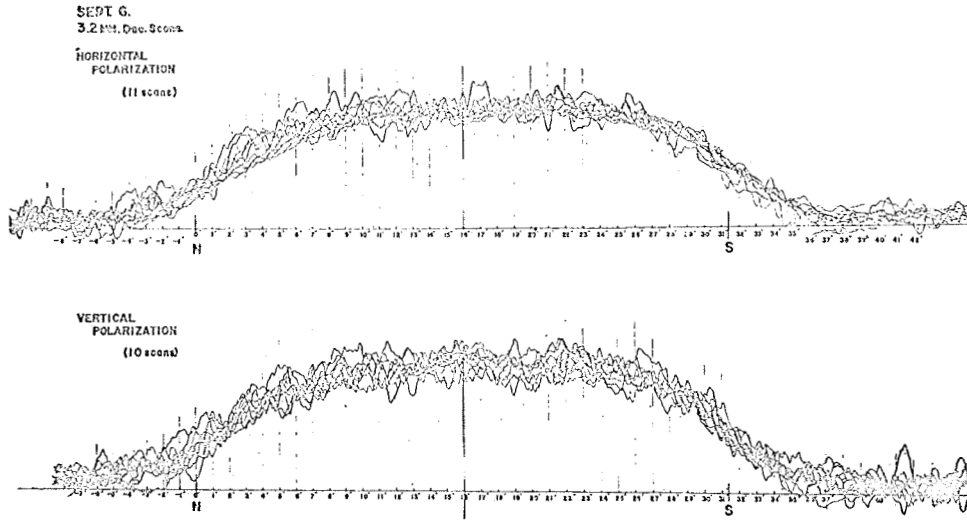

Fig.7. Scan curves for horizontal (upper) and vertical (lower) polarizations for 3.2 mm wavelength. Sept.6, 1968.

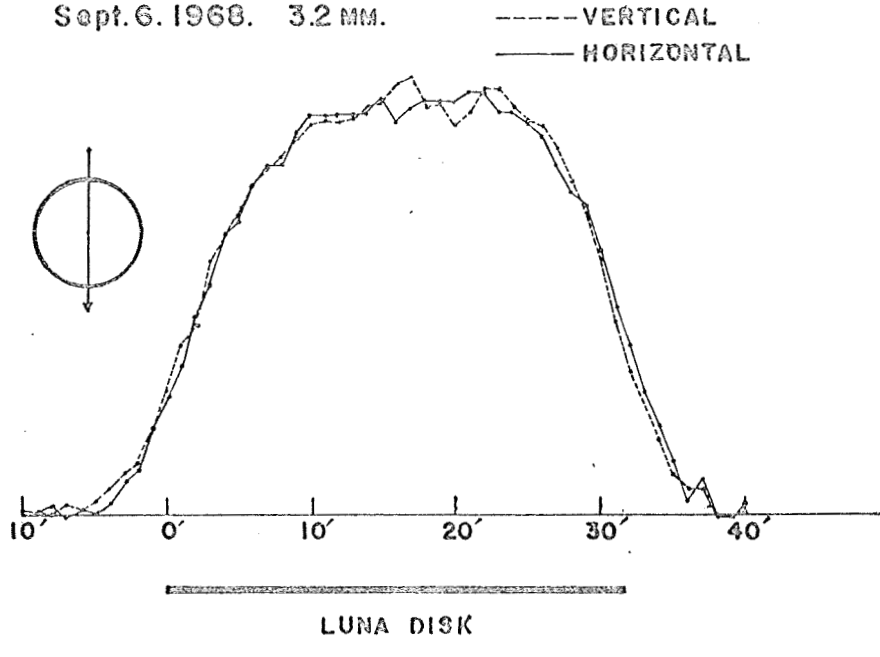

Fig.8. Averaged curves of Fig.7 for horizontal (———) and vertical (-----) polarizations.

el was made for the moon's semeidiameter of 15.5' while his ΔT_p values were obtained by the observation of the moon with semi-diameter of 16.4', which necessitated to make some manipulation in acquiring the average slope.

An observation of the moon was conducted on the night of September 3, 1968 using the 4.3 mm wavelength radiometer. At the time of this observation the radiometer was not in its best condition due to the excessive noisiness of its mixer, so that little could be hoped from the observation. In consequence of the processing of the data, however, at least the existence of the polarized component was found in it, and the result of this observation is shown in Figs.5 and 6. The measurement was carried out by means of declination scanning. In Fig.5 are shown two families of scan curves for the respective polarizations for the purpose of best visualizing the effects of receiver noise and atmospheric scintillations. In the family of curves for the horizontal polarization in Fig.5, a scatter of curves is seen at around 28' from the north limb, which has given rise to a bulge at the corresponding point in Fig.6. This scattering of the curves is due to the increase in receiver noise or atmospheric perturvations. Except the bulge in this part of the curve, the existence of the vertically polarized component may be concluded. However, the estimation of ΔT_p by the two curves in this figure may be overdoing since they are too fluctuant to do so.

Measurements of the polarization at 3.2 mm wavelength were carried out at 10-odd clear nights in the period August-September 1968. The result is shown in Figs.7 and 8. Fig.7 shows two families of declination csan curves for the respective polarizations as in the case of 4.3 mm wavelength measure-

ment. In Fig.8 are shown the resultant curves obtained by averaging eleven curves for horizontal polarization and ten curves for vertical polarization. As is seen in this figure it is hard to discriminate the polarized component, and hence we may conclude that the polarization should be very weak to be detected by the 3.2 mm wavelength radiometer used, i.e., $\Delta T_p < 1.5^{\circ}K$. If there should be the polarizized component cosiderably exceeding $1.5^{\circ}K$, which is approximately the minimum detectable temperature of the radiometer used in the measurement (NF $\leq$ 20dB, IFBW = 10 MHz, and integration time = 16 seconds), it would have been detected in the 10-odd nights' observations. Hence, it seems not to be an excess to conclude that the polarized component has the maximum temperature that does not exceed $1.5^{\circ}K$.

3. Lunar surface model

From the results of the observations so far introduced and by the aid of the results obtained at other wavelengths and radar measurements, a lunar surface model will be constructed.

If the depolarization effect at the 3.2 mm wavelength should be intrinsically related with the surface structure of the moon, we may be able to infer the scale of surface roughness by the joint use of the results obtained at other wavelengths.

In order to explain the depolarization effect of a wave, we will make the following assumptions: When the half size a of an undulation is much smaller than the wavelength of the wave, the efficiency of reflection and hence emission of the wave by the surface covered with an aggregation of such undulations would not decrease so much as compared with that of a smooth surface. As the size a approaches to a quarter wavelength of the probing wave, however, the efficiency becomes lower. This is just the

case of a paraboloid antenna whose efficiency is a function of surface roughness.

When the half size a exceeds a half wavelength of the wave and if the average slope of undulations be favorably oriented for the observer, the efficency becomes higher.

The effect of undulations with a certain size in the range $\lambda/2 > a > \lambda/4$ would, therefor, give rise to the lowest efficiency in reflecting or emitting the wave.

Thus, the depolarization effect at the 3.2 mm wavelength may be interpreted by the random scattering due to the surface covered with small scale undulations whose half size is distributed near 1 mm which is just in the range $\lambda/2 > a > \lambda/4$ for the 3.2 mm wave.

Kerr [5] has calculated the ratio of radar back-scattering cross section to geometrical cross section as a function of radius to wavelength for a sphere with infinite conductivity. Some of the radio cross sections after his result for various wavelengths of interest in observation for a=0.9 mm are shown in the following table.

Wavelength (mm)	8.6	6.0	4.3	3.2	2.2	1.5
Cross section (%)	100	310	205	23	140	140

As is seen in this table the radio cross section of a shpere with a radius of 0.9 mm is 23% of its geometrical cross section for the 3.2 mm wave, which indicates that the wave undergoes high random scattering by the element with a radius of 0.9 mm. Should the depolarization effect of the 3.2 mm wave be due to such elements perfused all over the lunar surface, they must have a very high conductivity since the calculation of Kerr was made for a sphere with infinite conductivity. Hence, it may be inferred that such elements as affect the scattering of the 3.2

mm wave should composed of some metalic substance.

Bastin [6] has found 4% polarization at a wavelength of 1.5 mm. The λ1.5 mm wave is efficiently reflected or emitted by the assumed roughness with a size distribution around 0.9 mm since the half wavelength of the wave is shorter than the average roughness scale of 0.9 mm.

These small scale roughness with a size distribution around 0.9 mm is perfused on the larger scale roughness ranging from several millimeters up to meters. The frequency distribution of the roughness scale may become larger as the roughness size becomes smaller.

This model surface structure as deduced from the millimetric observations thus far introduced is illustrated in Fig.9 below.

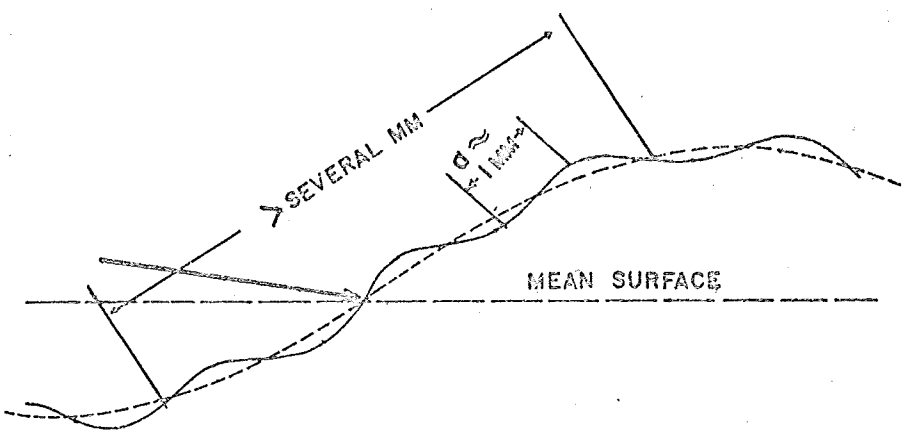

Fig.9. Surface structure as deduced from the millimetric observations.

Radarmetric exploration of the moon has supplied a good deal of information on the properties of the lunar surface. [e.g. 7]. Relative echo power vs. delay at various wavelengths is shown in Fig.10. As is readily seen in this figure, there is a distinct wavelength dependence in relative echo power, that is, the decrease of the relative echo power with increasing delay

becomes less as the sounding wavelength becomes shorter. This fact may be accounted for by considering the mannar of roughness scale distribution and the previously assumed surface structure in which the effect of the side of undulations favorably tilted toward the observer makes the apparent lunar shape deviate from a sphere to a somewhat flatter shape whose cross section may be describable by a curve something like an ellipse with its minor axis pointing at the observer. The ellipticity depends on wavelength due to the size distribution of surface roughness and also on the average slope of undulations, that is, the distribution of roughness and the average slope of undulations become greater as the scale of roughness reduces. This situation is illustrated in Fig.11. Should the angle between the normal at the point of observation and the direction of wave propagation, i.e., $\angle npO$,

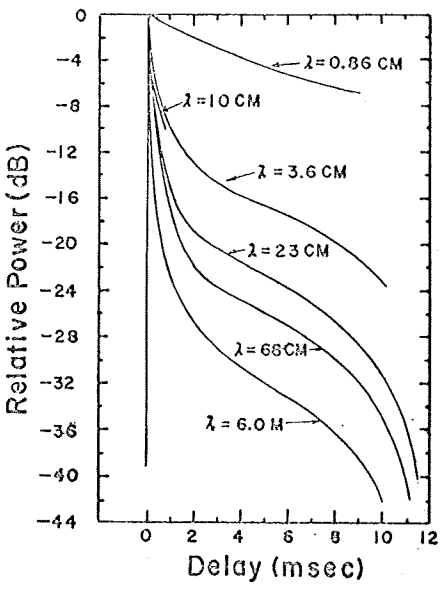

Fig.10. Relative echo power vs. delay at various wavelengths.

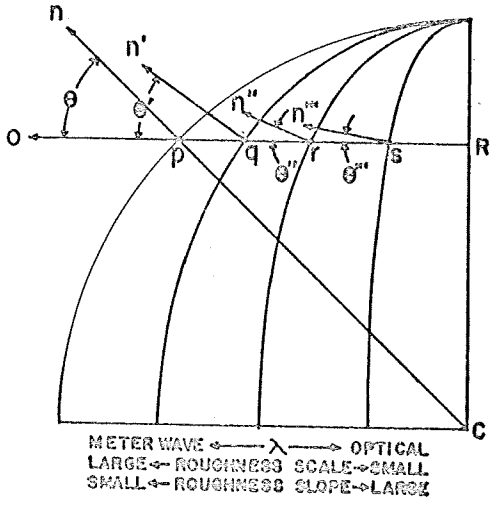

Fig.11. Wavelength dependence of ellipticity of apparent radio shape of the moon.

$\angle n' \neq 0$, $\angle n'' \neq 0$, ..., be related with the reflected power $P_{ref} \propto \cos\theta$, the reflectivity becomes larger as the ellipticity increases or as θ reduces to θ', θ'', θ''', and so on. Accordingly, at distance R from the disk center the reflected power would become larger (aside from the reduction of wave reflection due to the random scattering by small scale roughness) as the ellipticity becomes larger or wavelength reduces. This may be the account for the wavelength dependence of the relative echo power vs. delay.

Due to the present technical difficulties, radarmetric observation of the moon at wavelengths shorter than 8 mm has not yet been undertaken as far as this auther knows. Therefore, there is no knowing about the behavior of radar returns at short millimeter wavelengths. However, from the results of the observations at millimeter wavelengths so far introduced, it may be said that radar returns at 3.2 mm wavelength would show the least intensity compared with those at longer and shorter wavelengths.

4. Discussion and conclusion

In the measurements of the linear polarization of the lunar thermal emission, we put emphasis on the detection of the polarized component at 3.2 mm wavelength, and those at the 8.6 and 4.3 mm wavelengths were made as subsidiary means. Hence, quantitative discussions of the results obtained at the 8.6 and 4.3 mm wavelengths would necessarily be overdoing. Accordingly, only things we can state here are that the polarized component could be found down to the wavelength of 4.3 mm and that the polarization at the wavelength of 3.2 mm is very weak and may be less than 1.5°K which was the minimum detectable tempera-

ature of the 3.2 mm wavelength receiver at the time of the observation.

The radius distribution of grains around 0.9 mm as deduced from the results obtained by the observations at the millimeter wavelengths so far introduced calls for a very high conductivity of such elements since the calculation of Kerr was made by assuming an infinite conductivity of the sphere. It seems hard to believe that such very highly conductive grains should be the composent of the lunar surface materials. However, if the depolarization of the λ3.2 mm wave should be coming from the intrinsical nature associated with the surface structure, the size of the scatterer of the λ3.2 mm wave must come in the range $\lambda/2 > a > \lambda/4$, and hence the half size of the small scale roughness would not be far from the assumed value of 0.9 mm.

The method of measurements which was limited by the available functions of the radiometer was the source of difficulties. As was stated already, the polarized component ΔT_p was obtained by taking the difference between the vertical and horizontal antenna polarizations obtained in different scans. This method is subject to the variations in meteorological conditions. Consequently, at the 4.3 and 3.2 mm wavelengths even the average of 10 scans obtained under a favorable weather condition gave a fluctuant curve. Hence, the detection of the very weak polarization at the 3.2 mm wavelength by the method adopted was quite discouraging. However, there will be a fair chance of detecting the weak polarization if one employs a high speed polarization switch in the feed which enables one to measure the ΔT_p directly. Such a device as this will minimize the effects of meteorological variations, and then the detectable ΔT_p will be close to the minimum detectable temperature of the radi-

ometer.

The determination of the average slope of surface irregularities by means of the outward displacement of the maximum ΔT_p position as found in the 8.6 mm measurements depends critically on the accuracy of measurement. Hence, every possible source of error should be completely known before observations are made.

In the corroboratory measurements of the instrumental polarization a displacement of the antenna beam direction was found when the feed horn was rotated by 90° to change the antenna polarization. The effect was due to the eccentric alignment of the feed horn center by 0.5 mm from the true center, which introduced about 1.5' displacement of the beam direction every time the polarization was changed. This beam displacement was allowed for when the data were processed. However, even a slight position error introduced by the different antenna beam directions seems to have affected the accuracy considerably when the two curves for the individual polarizations were compared to obtain the ΔT_p. Hence, the estimated average slope of $8^\circ \pm 2^\circ$ from the result obtained at the 8.6 mm wavelength necessarily includes considerable uncertainty. Therefore, we may only suggest that the average slope may be determined by the outward displacement of the maximum ΔT_p position away from the theoretically expected position if the high accuracy could be secured. The high accuracy may be attainable by the use of a high speed polarization switch in the feed to obtain the ΔT_p directly and instantaneously as suggested in the case of the 4.3 and 3.2 mm wavelength measurements.

References

1. V. S. Troitsky, "On the theory of the radio emission of the moon," Astron. Zh., 31, No.6, 1954.

2. C. W. Tolbert, A. W. Straiton, and L. C. Krause, " A 16-foot diameter millimeter wavelength antenna system, its characteristics and its application," IEEE Trans. Antennas and Propagation, AP-13, No.2, March 1965.
3. J. R. Cogdell, " Calibration program for the 16-foot antenna," NASA Tech. Rep. NGL-006-69-1, January 1969.
4. J. M. Moran, Jr., " Radiometric observations of the moon near 1 cm wavelength," Dissertation submitted to the M.I.T., 1965.
5. D. E. Kerr, Propagation of Short Radio Waves, M. I. T. Radiation Laboratory Series, editted by L. N. Ridenour, McGraw-Hill Book Co., New York, 1951.
6. B. Ya. Losovskii, " Observations of the polarization of lunar radio radiation at the wavelength of 0.8 cm with high resolving power," Astronomicheskii Vestnik, 2 , No.3, July-September 1968.
7. I. V. Evans and G. H. Pettengil, " The scattering behavior of the moon at wavelengths of 3.6, 68 and 784 centimeters," J. Geophys. Res., 68, No.2, 1963.